SYNCHRONIZATION IN MULTILAYER NETWORKS: WHEN GOOD LINKS GO BAD *

IGOR BELYKH[†], DOUGLAS CARTER[‡], AND RUSSELL JETER[§]

Abstract. Many complex biological and technological systems can be represented by multilayer networks where the nodes are coupled via several independent networks. Despite its significance from both the theoretical and application perspectives, synchronization in multilayer networks and its dependence on the network topology remain poorly understood. In this paper, we develop a universal connection graph-based method which opens up the possibility of explicitly assessing critical multilayer-induced interactions which can hamper network synchronization. The method reveals striking, counterintuitive effects caused by multilayer coupling. It demonstrates that a coupling which is favorable to synchronization in single-layer networks can reverse its role and destabilize synchronization when used in a multilayer network. This property is controlled by the traffic load on a given edge when the replacement of a lightly loaded edge in one layer with a coupling from another layer can promote synchronization, but a similar replacement of a highly loaded edge can break synchronization, forcing a "good" link to go "bad." This method can be transformative in the highly active research field of synchronization in multilayer engineering and social networks, especially in regard to hidden effects not seen in single-layer networks.

Key words.

synchronization, multilayer networks, traffic load, network topology

AMS subject classifications. 34D06, 34D08, 34D20, 93E20

1. Introduction. Complex networks are common models for many systems in physics, biology, engineering, and the social sciences [59, 2, 46]. Significant attention has been devoted to algebraic, statistical, and graph theoretical properties of networks and their relationship to network dynamics (see a review [21] and references therein). The strongest form of network cooperative dynamics is synchronization which plays a significant role in the functioning of a wide spectrum of technological and biological networks [22, 25, 32, 35, 63, 50, 45, 24, 30, 43], including adaptive and evolving networks [4, 53, 52, 58, 56, 37, 8, 31, 51].

Despite the vast existence of literature on network dynamics and synchronization, the majority of research activities have been focused on oscillators connected through single-layer network (one type of coupling) [49, 33, 67, 20, 3, 65, 64, 16, 5, 66, 40, 11, 14, 61, 47, 44, 1, 68, 48]. However, in many realistic biological and engineering systems the units can be coupled via multiple, independent systems and networks. Neurons are typically connected through different types of couplings such as excitatory, inhibitory, and electrical synapses, each corresponding to a different circuitry whose interplay affects network function [39, 13]. Pedestrians on a lively bridge are coupled via several layers of communication, including people-to-people interactions and feedback from the bridge that can lead to complex pedestrian-bridge dynamics [60, 29, 15, 12]. In engineering systems, examples of independent networks include coupled grids of power

^{*}This work was supported by the National Science Foundation (USA) under Grants No. DMS-1909924 and No. DMS-1616345 and the U.S. Army Research Office under Grant No. W911NF-151-0267.

[†]Department of Mathematics and Statistics and Neuroscience Institute, Georgia State University, P.O. Box 4110, Atlanta, Georgia, 30302-410, USA (ibelykh@gsu.edu)

 $^{^{\}ddagger} Department of Mathematics and Statistics, Georgia State University, P.O. Box 4110, Atlanta, Georgia, 30302-410, USA$

 $[\]S$ Department of Mathematics and Statistics, Georgia State University, P.O. Box 4110, Atlanta, Georgia, 30302-410, USA and Department of Biomedical Informatics, Emory University, Atlanta, Georgia, USA

stations and communication servers where the failure of nodes in one network can lead to the failure of dependent nodes in another network [23]. Such interconnected networks can be represented by multiplex or multilayer networks [38, 19, 62, 18] which include multiple systems and layers of connectivity. Multilayer-induced correlations can have significant ramifications for the dynamical processes on networks, including the effects on the speed of disease transmission in social networks [26] and the role of redundant interdependencies on the robustness of multiplex networks to failure [54].

40 41

42

43

44

45

46

47

48

49

50 51

53

54

56 57

58

60

61 62

63

64

65

66

67 68

69

70

71

72 73 74

75

76

77 78

80

81

82 83

84 85

86

87

88

Typically, in single-layer networks of continuous time oscillators, synchronization becomes stable when the coupling strength between the oscillators exceeds a threshold value [49, 16]. This threshold depends on the individual oscillator dynamics and the network topology. In this context, a central problem is to determine the critical coupling strength necessary to guarantee the stability of synchronization. The master stability function [49] or the connection graph method [16, 5] are usually used to solve this problem in single-layer networks. Both methods reduce the dimensionality of the problem such that synchronization in a large, complex network can be predicted from the dynamics of the individual node and the network structure.

Synchronization in multilayer networks has been studied in [57, 36, 27, 69]; however, its critical properties and explicit dependence on intralayer and interlayer network structures remain poorly understood. This is in particular due to the inability of the existing eigenvalue methods, including the master stability function [49] to give detailed insight into the stability condition of synchronization as the eigenvalues, corresponding to connection graphs composing a multilayer network, must be calculated via simultaneous diagonalization of two or more connectivity matrices. Simultaneous diagonalization of two or more matrices is impossible in general, unless the matrices commute [57, 36]. A nice approach based on simultaneous block diagonalization of two connectivity matrices was proposed in [36]. This application of the eigenvaluebased approach allows one to reduce the dimensionality of a large network to a smaller network whose synchronization condition can be used to evaluate the stability of synchronization in the large network. For some network topologies, this technique yields a substantial reduction of the dimensionality; however, this reduction is less significant, in general. The reduced network typically contains weighted positive and negative connections, including self loops such that the role of multilayer network topologies and the location of critical edges that control synchronization remain difficult to eval-

In this paper, we report significant progress towards removing this obstacle to studying synchronization in multilayer networks. We develop a new general stability approach, called the Multilayer Connection Graph method, which does not depend on explicit knowledge of the spectrum of the connectivity matrices and can handle multilayer networks with arbitrary network topologies, which are out of reach for the existing approaches. An example of a multilayer network in this study is a network of Lorenz systems where some of the oscillators are coupled through the x variable (first layer), some through the y variable (second layer), and some through both (interlayer connections). Our Multilayer Connection Graph method originates from the connection graph method [16, 5] for single-layer networks; however, this extension is highly non-trivial and requires overcoming a number of technically challenging issues. This includes the fact that the oscillators from two x and y layers in the networks of Lorenz systems are connected through the intrinsic, nonlinear equations of the Lorenz system. As a result, multilayer networks can have drastically different synchronization properties from those of single-layer networks. In particular, our method shows that an interlayer traffic load on an edge (in the sense of paths utilizing this edge) is the crucial quantity which can be used to foster or hamper synchronization in a nonlinear fashion. For example, it demonstrates that replacing a link with a light interlayer traffic load by a stronger pairwise converging coupling (a "good" link) via another layer may lower the synchronization threshold and improve synchronizability. At the same time, such a replacement of a highly loaded link can make the network unsynchronizable, forcing the pairwise stabilizing "good" link to go "bad."

The layout of this paper is as follows. First, in Sec. 2, we present and discuss the network model. In Sec. 3, we start with a motivating example of how the replacement of some links in a multilayer network can improve or break network synchronization. In Sec. 4, we formulate the Multilayer Connection Graph method for predicting synchronization in multilayer networks. In Secs. 5-7, we show how to apply the general method to specific network topologies. In Sec. 8, a brief discussion of the obtained results is given. Finally, the Appendix contains the complete derivation of the general method. MATLAB code for algorithms used for calculating network traffic loads is given in the Supplement.

2. Network model and problem statement. We start with a network of n oscillators with three connectivity layers:

107 (2.1)
$$\frac{d\mathbf{x}_{i}}{dt} = \mathbf{F}(\mathbf{x}_{i}) + \sum_{j=1}^{n} c_{ij} P \mathbf{x}_{j} + \sum_{j=1}^{n} d_{ij} L \mathbf{x}_{j} + \sum_{j=1}^{n} g_{ij} M \mathbf{x}_{j}, \quad i = 1, ..., n,$$

where $\mathbf{x}_i = (x_i^1, ..., x_i^s)$ is the s state vector containing the coordinates of the i-th oscillator, $\mathbf{F}: \mathbb{R}^s \to \mathbb{R}^s$ describes the oscillators' individual dynamics, $C = (c_{ij})$, $D = (d_{ij})$, and $G = (g_{ij})$, are $n \times n$ Laplacian connectivity matrices with zerorow sums and nonnegative off-diagonal elements $c_{ij} = c_{ji}$, $d_{ij} = d_{ji}$, and $g_{ij} = g_{ji}$, respectively [16]. These connectivity matrices C, D, and G define three different connection layers (also denoted by C, D, and G with m, l, and q edges, respectively). The inner matrices P, L, and M determine which variables couple the oscillators within the C, D, and G layers, respectively. Without loss of generality, we will be considering oscillators of dimension s=3 with $\mathbf{x}_i=(x_i,y_i,z_i)$. Therefore, the C graph with the inner matrix P = diag(1,0,0) will correspond to the first-layer connections via x, the D graph with the inner matrix L = diag(0,1,0) will indicate the secondlayer connections via y, and the graph G with the matrix M = diag(0,0,1) will represent the third-layer connections via z. Overall, the oscillators of the network are connected through a combination of the three layers. The graphs are assumed to be undirected [16]. Oscillators, comprising the network (2.1), can be periodic or chaotic. As chaotic oscillators are difficult to synchronize, they are usually used as test bed examples for probing the effectiveness of a given stability approach. Although, we will show that the chaoticity of the oscillators is not important for the non-intuitive effects of multilayer synchronization. The oscillators used in the numerical verification of our stability method are chaotic Lorenz [41], chaotic double scroll oscillators [42], and periodic Hindmarsh-Rose oscillator models [34].

In this paper, we are interested in the stability of complete synchronization defined by the synchronization manifold $S = \{\mathbf{x}_1(t) = \mathbf{x}_2(t) = \dots = \mathbf{x}_n(t) = \mathbf{s}(t)\}$, where the synchronous solution $\mathbf{s}(t) = (x(t), y(t), z(t))$ is governed by the uncoupled individual oscillator. Our main objective is to determine a threshold value for the coupling strengths required for the stability of the synchronization manifold S. We seek to predict this threshold or the absence thereof in the general network (2.1) from synchronization in the simplest two-node network and graph properties of the multilayer network structures.

Based on their synchronization properties and a way they are coupled, oscillators can be divided into three main types [21]. Type I oscillators are capable of synchronizing globally and retaining synchronization for any coupling strengths exceeding the synchronization threshold. Most known oscillators, including the Lorenz, double scroll, and Hindmarsh-Rose oscillators belong to Type I systems. A much narrower Type II class of oscillators contains x-coupled Rössler systems [49] in which synchronization becomes stable but eventually looses its stability with an increase of coupling [33]. Type III oscillators cannot be synchronized by a given choice of coupling. In this work, we limit our consideration to the large class of Type I networks; however, an extension of our method to Type II networks could be performed with moderate effort and remains a subject of future study.

3. A motivating example and a puzzle. To illustrate the complexity of assessing multilayer connections and their controversial role in fostering or hindering synchronization, we begin with simple two-layer networks of chaotic Lorenz oscillators, depicted in Fig. 1(a-c). The two-layer networks are chosen as a minimum model which can exhibit counterintuitive effects due to the multilayer structure. For the two-layer networks of Lorenz oscillators, the vector equation (2.1) can be written in a more reader-friendly scalar form:

$$\dot{x}_{i} = \sigma(y_{i} - x_{i}) + \sum_{j=1}^{n} c_{ij}x_{j},
\dot{y}_{i} = rx_{i} - y_{i} - x_{i}z_{i} + \sum_{j=1}^{n} d_{ij}y_{j},
\dot{z}_{i} = -bz_{i} + x_{i}y_{i}, \quad i = 1, ..., n,$$

where the connectivity matrix $C = (c_{ij})$ describes the topology of x connections (black edges in Fig. 1(a-c)), and matrix $D = (d_{ij})$ describes the location of one y edge (blue or red edge). Notice the absence of the z coupling and, therefore, of the third layer G. The parameters of the individual Lorenz oscillator are standard: $\sigma = 10$, r = 28, and b = 8/3. The strengths of the x and y coupling are homogeneous $(c_{ij} = c, d_{ij} = d)$ and varied uniformly (c = d).

We are interested in the question of how the replacement of an x edge in the network of Fig. 1(a) with a y edge can affect synchronization. To address this question, we first need to understand synchronization properties of two-node single-layer networks of x-coupled and y-coupled Lorenz systems. It is well-known that if the coupling in a single-layer network (3.1) with either all x or all y connections exceeds a critical threshold, then synchronization becomes stable and persists for any c > c* and $d > d^*$, respectively [16].

Calculated numerically 1 , these coupling thresholds are $c^* \approx 3.81$ for the two-node x-coupled network and $d^* \approx 1.42$ for the y-coupled network. As the synchronization threshold d^* is significantly lower, one could expect that replacing an x edge with a presumably better converging y coupling improves synchronization. This is true for the network in Fig. 1(b) when x edge 5-6 is replaced with a y edge, yielding a minor reduction in the synchronization threshold from $c^* \approx 17.94$ in the single-layer x-coupled network in Fig. 1(a) to $c^* \approx 17.74$ in the multilayer network in Fig. 1(b). The network of Fig. 1(c) replaces an x edge with a y edge, and naturally we would

¹Numerical calculations of coupling thresholds c^* and d^* throughout this paper were performed using an eighth-order Runge-Kutta method with step size h = 0.001. Initial conditions for (x_i, y_i, z_i) are chosen uniformly at random within the unit hypersphere. Synchronization has been defined as the sum of all difference variables less than 0.00001.

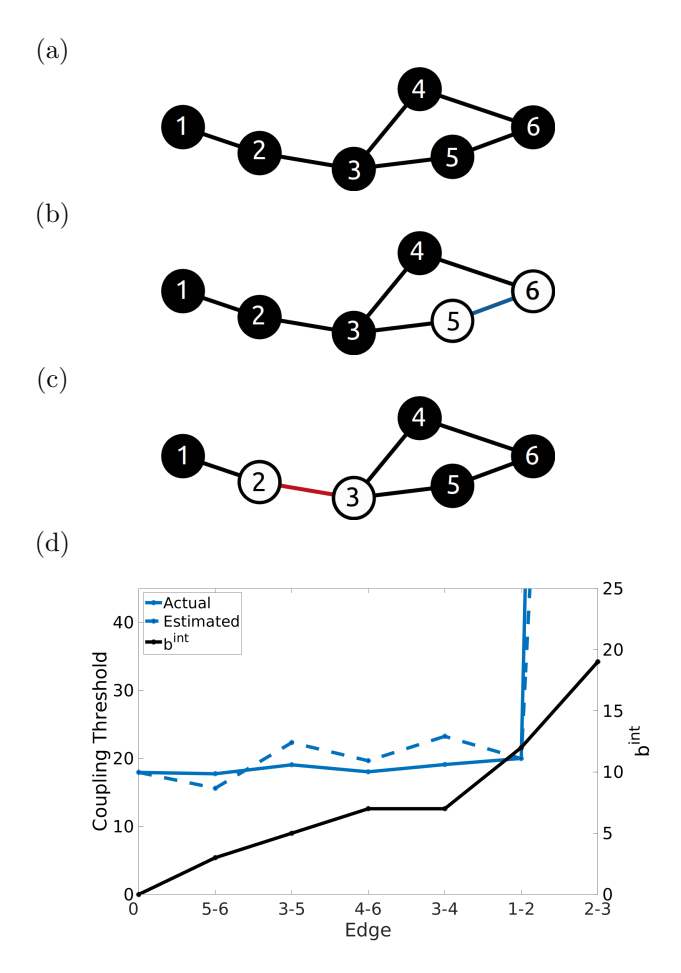


FIG. 1. The puzzle: why do "good" links go "bad"? Synchronization in six-node networks of Lorenz systems (3.1). (a) Single-layer network, with all x edges (black). (b) The replacement of x edge 5-6 with a presumably better converging y coupling (blue) improves synchronization, as expected (see (d)). (c) A similar replacement of x edge 2-3 with a y edge (red) makes synchronization impossible by pushing the threshold to infinity (see (d)). (d). Systematic study of the coupling threshold c^* as a function of the y edge location that replaces an x edge in the original x-coupled network (a). The blue solid line indicates numerically calculated thresholds. The black solid line depicts the interlayer traffic b^{int} for the respective y edge. Note a significant increase of b^{int} that causes the network to become unsynchronizable as predicted by the method. The predicted coupling thresholds (blue dotted line) are computed from (4.12) using the exponential fit in Fig. 3 and scaling factors $\beta = 0.3517$ and $\gamma = 0.7180$.

expect this to improve synchronization. Surprisingly, the contrary is true – this action makes the network unsynchronizable (see the coupling threshold jumping to infinity in Fig. 1(d)).

What is the origin of this counterintuitive effect? Why do edges in a multilayer network reverse their stabilizing roles depending on the edge location whereas they are well behaved in single-layer networks? The connectivity matrices for x and y coupling in the networks in Fig. 1(b) and Fig. 1(c) do not commute and, therefore, the predictive power of the master stability function based methods [57, 36, 27] is severely impaired. This puzzle calls for an explanation and utlimately motivates the development of an effective, general method for assessing the stability of synchronization in

multilayer networks.

In the following, we will develop such a method that identifies the location of critical interlayer links which control stable synchronization and reveals its explicit dependence on an interlayer traffic load on a given edge.

- 4. Multilayer Connection Graph Method. In this section, we present the analytical method and then derive its practical numerically-assisted version which represents an effective approach to assessing the role of critical links from the knowledge of two-node networks and graph characteristics of the underlying network topology. We then demonstrate how to apply the method to specific network configurations.
- **4.1.** Analytical method: conservative bounds. To formulate the main theorem, we first need to make several assumptions and introduce important quantities. Towards assessing the role of the individual oscillator and type of pairwise coupling within each layer, we should consider three types of the two-node networks (2.1) which are only coupled through one variable. These are x-coupled, y-coupled, and z-coupled networks. For each of these two-node networks with coupling strengths $c_{12} = c_{21} = c$, $d_{12} = d_{21} = d$, and $g_{12} = g_{21} = g$, respectively, we assume that there exists a threshold value, c^* for the x-coupled, d^* for the y-coupled, and g^* for the z-coupled network, which guarantees the global stability of synchronization for any coupling strength exceeding the threshold values. This assumption implies that each x, y, and z coupling belongs to the Type I class of coupled oscillators. For mathematical convenience, we introduce the corresponding constants $a_x = 2c^*$, $a_y = 2d^*$, and $a_z = 2g^*$ which are the double coupling strengths that are sufficient for the synchronization in the x-, y-, and z-coupled two-node networks, respectively. Rigorous upper bounds on the double coupling strength a_x explicit in parameters of the individual oscillator have been previously derived for coupled Lorenz oscillators [16], double-scroll Chua oscillators [17], driven nonlinear pendulums [10], and Hindmarsh-Rose neuron models [11].

We also consider the two-node network with all x, y, and z coupling and introduce the triple $(\omega_x, \omega_y, \omega_z)$ as a combination of the double coupling strengths c, d, and g that guarantee the synchronization in the xyz-coupled two-node network. These constants are such that $\omega_x \leq a_x$, $\omega_y \leq a_y$, and $\omega_z \leq a_z$, where equality relates to the previous case of the two-node network coupled through one variable. Obviously, there are different possible combinations of ω_x , ω_y , and ω_z to choose from; however, one should pick a combination that balances out the stability conditions. This point will be discussed in the next subsection in more detail.

Similarly to the connection graph method for single-layer networks [16], we also need to introduce graph theoretical quantities that characterize the total length of the chosen paths that go through each edge of the three-layer network (2.1). This is done by choosing a set of paths $\{|P_{ij}| \ i, j=1,...,n,\ j>i\}$, one for each pair of nodes i,j and then determining their lengths $|P_{ij}|$, the number of edges in each P_{ij} . We then partition the chosen paths into two categories such as (i) the paths within one layer that only contain edges of one coupling type, for example, x edges and (ii) the paths that are composed of two or three types of edges, for example, x and y edges. Starting from the first x layer C, we calculate the following quantity for each x edge k = 1,...,m

232 (4.1)
$$b_k^x = \sum_{j>i; k \in P_{ij} \in C}^n |P_{ij}|.$$

Here, b_k^x is the sum of the lengths of all chosen paths P_{ij} between any pair of nodes

i and j which belong to the x layer C and go through a given x edge k. These paths are entirely composed of x edges. Similarly, we introduce

236 (4.2)
$$b_k^y = \sum_{j>i; k \in P_{ij} \in D}^n |P_{ij}|, k = 1, ..., l, b_k^z = \sum_{j>i; k \in P_{ij} \in G}^n |P_{ij}|, k = 1, ..., q$$

as the sums of all chosen paths P_{ij} between any pair of nodes i and j which entirely belong to the y(z) layer and go through a given y(z) edge k. Finally, we introduce the quantity

240 (4.3)
$$b_k^{int} = \sum_{j>i; k \in P_{ij}: (i,j) \notin C, D, G} |P_{ij}|$$

241

242

243

244

245

246

247

248

249

250

251252

253

254

255

256

as the sum of the lengths of all chosen paths P_{ij} which pass through a given edge k and are composed from more than one type of edges. These are the paths between pairs of nodes i and j which belong to two different layers. For example, a path between two nodes from x and y layers is typically composed of x and y edges but may also contain z edges as the path from a node from the x layer may have to pass through the z layer to reach the y layer.

In terms of traffic networks, the graph theoretical quantities b_k^x , b_k^y , b_k^z , and b_k^{int} represent the total lengths of the chosen roads that go through a given edge k which can be loosely analogized as a busy street. Therefore, we refer to them as "traffic" loads. In this view, the quantity b_k^{int} is a traffic load on edge k, caused by interlayer travelers.

Having introduced the main constants a_x , a_y , a_z , ω_x , ω_y , ω_z , related to the two-node network (2.1) and the traffic loads b_k^x , b_k^y , b_k^z , and b_k^{int} , we can formulate the Multilayer Connection Graph Method. For convenience, we use the notations $c_k = c_{i_k,j_k}$, $d_k = d_{i_k,j_k}$, and $g_k = g_{i_k,j_k}$ which indicate the coupling strengths of the corresponding edges k on the x, y, and z layer graphs, respectively.

THEOREM 4.1 (sufficient conditions). Complete synchronization in the threelayer network (2.1) is globally stable if for each edge k

$$c_{k} > \frac{1}{n} \left\{ a_{x} \cdot b_{k}^{x} + \omega_{x} \cdot b_{k}^{int} + \alpha_{x}^{k} \right\}, \ k = 1, ..., m,$$

$$d_{k} > \frac{1}{n} \left\{ a_{y} \cdot b_{k}^{y} + \omega_{y} \cdot b_{k}^{int} + \alpha_{y}^{k} \right\}, \ k = 1, ..., l,$$

$$g_{k} > \frac{1}{n} \left\{ a_{z} \cdot b_{z}^{z} + \omega_{z} \cdot b_{k}^{int} + \alpha_{z}^{k} \right\}, \ k = 1, ..., q,$$

where the constants α_x^k , α_y^k , and α_z^k are chosen large enough such that they can globally stabilize the auxiliary stability systems written for the difference variables that correspond to an edge $k: \mathbf{X}_k = \mathbf{X}_{ij} = \mathbf{x}_j - \mathbf{x}_i$:

$$\begin{array}{rcl}
\text{for } \alpha_x^k : \dot{\mathbf{X}}_k &= \left[\int_0^1 D\mathbf{F}(v\mathbf{x}_j + (1-v)\mathbf{x}_i) dv \right] \mathbf{X}_k + \\
\omega_y b_k^{int} L\mathbf{X}_k + \omega_z b_k^{int} M\mathbf{X}_k - (a_x + \alpha_x^k) P\mathbf{X}_k, \\
\text{264}
\end{array}$$

 $\begin{array}{rcl}
\text{265} \quad (4.6) & \text{for } \alpha_y^k : \quad \dot{\mathbf{X}}_k & = \left[\int_0^1 D\mathbf{F}(v\mathbf{x}_j + (1-v)\mathbf{x}_i) dv \right] \mathbf{X}_k + \\
& \omega_x b_k^{int} P\mathbf{X}_k + \omega_z b_k^{int} M\mathbf{X}_k - (a_y + \alpha_y^k) L\mathbf{X}_k, \\
\text{266} & & & & & & & \\
\end{array}$

$$\begin{array}{rcl}
\text{for } \alpha_z^k : \dot{\mathbf{X}}_k &= \left[\int_0^1 D\mathbf{F}(v\mathbf{x}_j + (1-v)\mathbf{x}_i) dv\right] \mathbf{X}_k + \\
\omega_x b_k^{int} P\mathbf{X}_k + \omega_y b_k^{int} L\mathbf{X}_k - (a_z + \alpha_z^k) M\mathbf{X}_k, \\
\end{array}$$

where $D\mathbf{F}$ is the $s \times s$ Jacobian matrix of \mathbf{F} and the notation $\int_{0}^{1} D\mathbf{F}(v\mathbf{x}_{j} + (1-v)\mathbf{x}_{i})dv$ represents the mean value theorem applied to the difference of vector functions $\mathbf{F}(\mathbf{x}_{j}) - \mathbf{F}(\mathbf{x}_{i})$.

Proof. The proof closely follows the notations and steps in the derivation of the connection graph method [16] for single-layer networks up to a point where the stability argument becomes drastically different and yields the new terms $\omega_x b_k^{int}$, $\omega_y b_k^{int}$, and $\omega_z b_k^{int}$ which play a pivotal role in synchronization of multilayer networks. The complete proof is given in the Appendix.

Remark 1. It is important to notice that positive terms $+\omega_y b_k^{int} L \mathbf{X}_k$ and $+\omega_z b_k^{int} M \mathbf{X}_k$ in the equation (4.5), $+\omega_x b_k^{int} P \mathbf{X}_k$ and $+\omega_z b_k^{int} M \mathbf{X}_k$ in (4.6), and $+\omega_x b_k^{int} P \mathbf{X}_k$ and $+\omega_y b_k^{int} L \mathbf{X}_k$ in (4.7) play a destabilizing role such that a heavily loaded edge with a high b_k^{int} can represent a potential problem for making the systems (4.5)-(4.7) stable at all. This observation has dramatic consequences for synchronization in specific multilayer networks described in the following sections and also is a key to solving the puzzle of Fig. 1.

Remark 2. If all x, y, and z connection graphs are connected such that all oscillators are coupled via all three graphs, the stability of synchronization can be simply assessed by applying the connection graph method [16] for each of the x, y, and z connected graphs and combining the three conditions as follows: $c_k + d_k + g_k > \frac{1}{n} \{a_x b_k^x + a_y b_k^y + a_z b_k^z\}$ (cf. the condition (9.25) in the Appendix). As a result, one should not expect the effects due to the multilayer coupling discussed in the motivating example.

Remark 3. The stability criterion (4.4) can be directly extended to oscillators of higher dimensions and/or multiple connection layers. For example, in the case of a four-layer network of five-dimensional oscillators with variables x, y, z, u, w coupled through the first four variables x, y, z, u, the stability criterion (4.4) should be simply extended by adding a similar inequality for the coupling strength corresponding to edges from the fourth additional layer with a_u , b_k^u , ω_u , and α_u^k defined similarly to the constants corresponding to the x, y, and z variables. The remaining uncoupled variable w does not play an explicit role in the stability criterion; however, it affects (i) the choice of values for ω_x , ω_y , ω_z , ω_u required for synchronization in the two node xyzu-coupled network and (ii) the values of $\alpha_x^k, \alpha_y^k, \alpha_z^k, \alpha_u^k$ via the increased dimensionality of the four auxiliary systems similar to (4.5)-(4.7).

While the stability criterion (4.4) is completely rigorous, the theoretical bounds derived by using Lyapunov functions may give large overestimates on the threshold coupling strength. As a result, bounds of the constants α_x^k , α_y^k , and α_z^k that are required to stabilize the auxiliary systems (4.5)-(4.7) may be too conservative or not exist.

In the following subsection, we take a more practical route towards developing a semi-analytical approach which evaluates local stability of synchronization. This computer-assisted version of the method combines numerically calculated constants associated with the individual oscillator dynamics with graph theoretical quantities such as traffic loads. In this way, this method combines the best of both worlds – the master stability function and the developed connection graph-based method – and becomes an effective, predictive tool for the general multilayer network (2.1) where the synchronization threshold or the absence thereof can be deduced from the properties of the individual oscillators and the network topologies of the connection layers.

4.2. Numerically-assisted multilayer connection graph method. For the sake of clarity, we consider the general network (2.1) with only two connection layers C and D. Its general vector equation (2.1) can be re-written in the scalar form:

$$\dot{x}_{i} = F(x_{i}, y_{i}, z_{i}) + \sum_{j=1}^{n} c_{ij}x_{j},
\dot{y}_{i} = Q(x_{i}, y_{i}, z_{i}) + \sum_{j=1}^{n} d_{ij}y_{j},
\dot{z}_{i} = R(x_{i}, y_{i}, z_{i}), \quad i = 1, ..., n,$$

316 317

318

321

322

323

324

331

333

334 335

336

337

338

339

341

342

343

345

346

347

348

349

350

351

352

353

354

355

with $\mathbf{x}_i = (x_i, y_i, z_i)$ and $\mathbf{F} = (F(x_i, y_i, z_i), Q(x_i, y_i, z_i), R(x_i, y_i, z_i)).$ 320

The stability conditions (4.4) can be directly adapted to the two-layer network (4.8) by only considering the two first inequalities for c_k and d_k with α_x^k and α_y^k calculated via the auxiliary systems (4.5) and (4.6) without the terms containing the projection matrix M. Computer-assisted derivation of the stability conditions (4.4)for the network (4.8) is a four-step process which can be summarized as follows.

Step 1: Synchronization thresholds in a two-node network. 326

327 Calculate a stability diagram for synchronization in the simplest two-node xy-coupled network with $c_{12} = c_{21} = c$ and $d_{12} = d_{21} = d$, using the variational equations for 328 infinitesimal transverse perturbations $\xi = x_2 - x_1$, $\eta = y_2 - y_1$, and $\zeta = z_2 - z_1$: 329

330 (4.9)
$$\dot{\xi} = F_x(\mathbf{s})\xi + F_y(\mathbf{s})\eta + F_z(\mathbf{s})\zeta - 2c\xi
\dot{\eta} = Q_x(\mathbf{s})\xi + Q_y(\mathbf{s})\eta + Q_z(\mathbf{s})\zeta - 2d\eta
\dot{\zeta} = R_x(\mathbf{s})\xi + R_y(\mathbf{s})\eta + R_z(\mathbf{s})\zeta.$$

Here, the partial derivatives form the Jacobian $D\mathbf{F}$ as in (4.5) and are evaluated at the synchronous solution $\mathbf{s}(t) = (x(t), y(t), z(t)).$

Use the stability diagram to determine threshold coupling strengths that guarantee stable synchronization in (i) the two-node x-coupled network with $c^* = a_x/2$ and d=0; (ii) the two-node y-coupled network with $d^*=a_y/2$ and c=0; and (iii) the two-node xy network with $c^* = \omega_x$ and $d^* = \omega_y$ (see Fig. 2). The new constants a_x and a_y are double coupling strengths required for synchronization in the two xcoupled and y-coupled oscillators (4.8), respectively. Note that different combinations of $c = \omega_x$ and $d = \omega_y$ in the xy-coupled network can yield stable synchronization. The choice of the pair (ω_x, ω_y) is somewhat arbitrary; however, it dictates the choice of constants in the stability diagrams in Step 3. It is often a good idea to choose ω_x and ω_y such that both are non-zero and lie somewhere in the middle range of (ω_x, ω_y) to balance out the stability conditions in Step 4.

Step 2: Graph theoretical quantities and traffic loads. 344

This calculation is similar to that of the connection graph method for single-layer networks [16], except that the traffic load should be partitioned into three groups: intralayer traffic loads b_k^x and b_k^y within the x and y layer, respectively, and interlayer traffic load b_k^{int} between the layers. To do so, we first choose a set of paths $\{|P_{ij}| \ i,j=1,...,n,\ j>i\}$, one for each pair of vertices i,j, and determine their lengths $|(P_{ij})|$, the number of edges in each P_{ij} . Then, for each edge k of the x(y)layer graph, we calculate the sum b_k^x (b_k^y) of the lengths of all P_{ij} that are composed of only x(y) edges and pass through k. We repeat the same procedure to calculate the sum b_k^{int} of the lengths of all P_{ij} that contain both x and y edges and pass through k. These constants depend on the choice of the paths P_{ij} . Usually, one uses the shortest path from vertex i to vertex j. Sometimes, however, a different choice of paths can lead to lower bounds [11]. In the following section, we will walk the reader through a

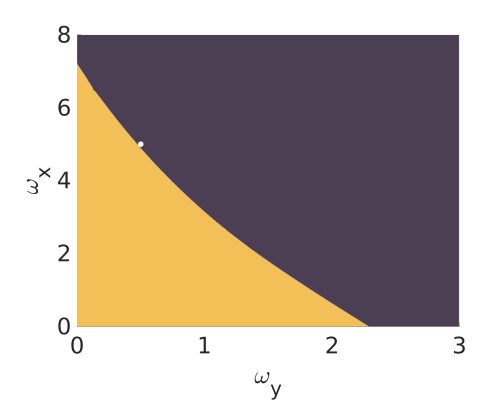


Fig. 2. Stability of synchronization in a two-node network of xy-coupled Lorenz systems (3.1) as a function of the x coupling, ω_x and the y coupling, ω_y . Yellow depicts instability (non-zero synchronization error) and purple depicts stability (zero synchronization error). The white dot indicates the pair (ω_x, ω_y) used in the predictions shown in Fig. 1(d) and Fig. 4(c).

detailed calculation of traffic loads b_k^x , b_k^y , and interlayer b_k^{int} in the six-node networks of Fig. 1.

Note that Steps 1 and 2 are quite similar to those one takes when applying the master stability function or the connection graph method to single-layer networks. That is, one identifies the role of the single node (via the calculation of the Lyapunov exponents in Step 1) and the role of the underlying network topology (via the calculation of the traffic loads in Step 2).

The next step is a new component of the method which does not follow from the connection graph method for single-layer networks and allows one to reveal and explain the surprising phenomena, including the previously described puzzle due to the multilayer network structure.

Step 3: Auxiliary stability diagrams to determine α_x^k and α_y^k .

358

359

360

361

362 363

364 365

366

367

368

374

375 376

377

378

379

380

The auxiliary global stability systems (4.5) and (4.6) for each edge k can be written 369 for the local stability in terms of the variational system (4.9) as follows: 370

$$\dot{\xi} = F_x(\mathbf{s})\xi + F_y(\mathbf{s})\eta + F_z(\mathbf{s})\zeta - (a_x + \alpha_x^k)\xi
\dot{\eta} = Q_x(\mathbf{s})\xi + Q_y(\mathbf{s})\eta + Q_z(\mathbf{s})\zeta + A\eta
\dot{\zeta} = R_x(\mathbf{s})\xi + R_y(\mathbf{s})\eta + R_z(\mathbf{s})\zeta,$$

372 (4.11)
$$\dot{\xi} = F_x(\mathbf{s})\xi + F_y(\mathbf{s})\eta + F_z(\mathbf{s})\zeta + B\xi
\dot{\eta} = Q_x(\mathbf{s})\xi + Q_y(\mathbf{s})\eta + Q_z(\mathbf{s})\zeta - (a_y + \alpha_y^k)\eta
\dot{\zeta} = R_x(\mathbf{s})\xi + R_y(\mathbf{s})\eta + R_z(\mathbf{s})\zeta.$$

where $A = \beta \omega_y b_k^{int}$ and $B = \beta \omega_x b_k^{int}$ with a scaling parameter β to be determined. As in (4.4), the auxiliary stability system (4.10) corresponds to the differences between the nodes connected by an x edge, and (4.11) corresponds to the differences between nodes coupled via a y edge. If the connection layers overlap and the same nodes are connected through both x and y edges, then the auxiliary systems (4.10) and (4.11) should be applied to the corresponding x and y edges independently. Their contributions will then appear in the general stability conditions (see Step 4) for c_k and d_k for the same edge k.

Notice that $\alpha_x^k \left[\alpha_y^k \right]$ must be large enough to stabilize (4.10) [(4.11)] in the presence of the destabilizing term $+A\eta$ [+B\xi]. While $a_x=2c^*$, $a_y=2d^*$, ω_x , and ω_y are chosen and fixed in Step 1 (cf. Fig. 2), the traffic load b_k^{int} on a given edge k (which is determined in Step 2) controls the choice of α_x^k and α_y^k . Thus, if the edge is highly loaded with a large b_k^{int} making A large, then the contribution of the destabilizing term $+A\eta$ in the η -equation of system (4.10) cannot always be compensated by increasing $\alpha_x^k \xi$ in the ξ -equation. Therefore, the auxiliary system (4.10) can become unstable, independently of how large the stabilization coefficient α_x^k is. The same argument relates to the destabilization of the auxiliary system (4.11) via the positive term $+B\xi$.

It is important to emphasize that diagrams for the local stability of the two three-dimensional auxiliary systems (4.10) and (4.11) can be calculated once and then be used to identify threshold values for constants α_x^k and α_y^k for each edge k with a given traffic load b_k^{int} . To do so, one should calculate the stability diagram for the threshold value of $\alpha_x^k \left[\alpha_y^k\right]$ necessary to stabilize the systems (4.10) [(4.11)] as a function of parameter $A\left[B\right]$. When generating the diagrams, A and B should be used as free parameters, thereby treating $\beta \omega_y b_k^{int}$ and $\beta \omega_x b_k^{int}$ as single, aggregated control parameters. As a result, the threshold value for $\alpha_x^k \left[\alpha_y^k\right]$ required to stabilize the auxiliary system (4.10) [(4.11)] for a given edge k with b_k^{int} can simply be taken from the diagram much in the vein of the master stability function [49] (see Fig. 3).

Because of the Cauchy-Schwarz inequality used in the derivation of the analytical method (see the Appendix), b_k^{int} provides an overestimate for the terms added to the auxiliary system, we have added the scaling factor $0 < \beta \le 1$ to b_k^{int} in A and B to compensate for this overestimate. To choose the scaling factor, one can use one point on the threshold value curve for α_k^x or α_y^d (see Fig. 3).

Step 4: Putting pieces together. Using the constants identified in Steps 1-3, we can predict synchronization coupling thresholds for the local stability of synchronization in the multilayer network (4.8) via the numerically assisted modification of (4.4):

$$c_k > \frac{1}{n} \left[\gamma_1 a_x \cdot b_k^x + \beta \omega_x \cdot b_k^{int} + \alpha_x^k \right],$$

$$d_k > \frac{1}{n} \left[\gamma_2 a_y \cdot b_k^y + \beta \omega_y \cdot b_k^{int} + \alpha_y^k \right].$$

Notice the presence of additional scaling factors γ_1 and γ_2 which are chosen to compensate for the conservative nature of b_k^x and b_k^y as in the connection graph stability method for single-layer networks [16, 5]. γ_1 (γ_2) scales down the term $\frac{a_x}{n}$ [$\frac{a_y}{n}$] to match the coupling needed to synchronize the network (4.8) which contains only x edges (y edges) with $b_k^{int} = 0$.

In the case of two-layer networks (4.8) with uniform coupling within each layer $c_k = c$ and $d_k = d$, the stability criterion (4.12) should be satisfied for $c > \max_k c_k$ and $d > \max_k d_k$. The auxiliary systems (4.10) and (4.11) are typically quite sensitive to changes in A and B, resulting in large α_x^k or α_y^k that dominate the other two terms in the stability condition (4.12). Therefore, it is often sufficient to check the stability condition (4.12) for only two edges (one from each x and y layers) which have maximum interlayer traffic loads among the edges of the corresponding layers. These maximum traffic loads $\max_k b_k^{int}$ yield the maximum values of α_x^k or α_y^k that in turn maximize the threshold values c and d.

Note that the principal new component of our method is the use of the auxiliary stability diagrams which indicate how the dynamics of the given oscillator comprising the network can be stabilized via one variable corresponding to one connection layer when an instability is introduced via the other variable from another connection layer. These stability diagrams are calculated for the three-dimensional variational systems (4.10) and (4.11) and allow for predicting the synchronization threshold in a large multilayer network by using purely graph theoretical quantities such as traffic loads. In this sense, these diagrams can be viewed as a hybrid of the master stability function and the connection graph method, applied to multilayer networks.

In the following section, we will walk the reader through the implementation of the stability conditions (4.12) for specific two-layer networks and illustrate their implications for the stability of synchronization.

5. Application of the method: solving the puzzle. Armed with the predictive method, we first return to the puzzle to better understand synchronization properties of the six-node networks of Lorenz oscillators (3.1) from Fig. 1. Below we follow the four steps of how our numerically-assisted method can be applied to these networks.

441 Step 1: Calculate a_x , a_y , ω_x , and ω_y .

428

443

462

Consider the simplest two-node network (3.1) with both x and y coupling: $c_{12} = c_{21} = c$ and $d_{12} = d_{21} = d$. Use the variational equations (4.9) to determine threshold coupling strengths that guarantee stable synchronization in (i) the two-node x-coupled network with $c^* = a_x/2$ and d = 0; (ii) the two-node y-coupled network with $d^* = a_y/2$ and c = 0; and (iii) the two-node xy network with $c^* = \omega_x$ and $d^* = \omega_y$.

The numerically calculated thresholds for the x-coupled and y-coupled two-node network (3.1) reported in Sec. 3 are $c^* \approx 7.62/2$ and $d^* \approx 2.84/2$, respectively. This yields the double coupling strength constants $a_x = 7.62$ and $a_x = 2.84$ to be used in (4.12).

Note that different combinations of $c = \omega_x$ and $d = \omega_y$ in the xy-coupled network yield stable synchronization (see Fig. 2). Without loss of generality, we choose $c = \omega_x = 5$ and $d = \omega_y = 0.5$ as a point on the stability boundary in Fig. 2 and keep these values fixed for the prediction of the synchronization threshold in larger two-layer networks (3.1) with arbitrary topologies.

Step 2: Calculate traffic loads b_k^x , b_k^y , and b_k^{int} .

We use the six-node multilayer network of Fig. 1(b) as an example for calculating intralayer traffic loads b_k^x and b_k^y within the x and y layer, respectively, and interlayer traffic load b_k^{int} between the layers. To compute all of the paths that pass through a given edge, it is recommended that the reader algorithmically finds the shortest path between every pair of oscillators, and take note of the paths that go through edge k and differentiate the paths that entirely belong to only the x or y layers and the ones that contain a combination of x and y edges. As a result, we can find each edge's traffic loads as follows

$$b_{12}^{x} = |P_{12}| + |P_{13}| + |P_{14}| + |P_{15}| + |P_{16}| = 1 + 2 + 3 + 3 + 4 = 13,$$

$$b_{23}^{x} = |P_{13}| + |P_{14}| + |P_{15}| + |P_{16}| + |P_{23}| + |P_{24}| + |P_{25}| + |P_{26}| = 20,$$

$$b_{34}^{x} = |P_{14}| + |P_{16}| + |P_{24}| + |P_{26}| + |P_{34}| = 15$$

$$b_{35}^{x} = |P_{15}| + |P_{25}| + |P_{35}| = 6, \quad b_{46}^{x} = |P_{16}| + |P_{46}| = 5,$$

$$b_{56}^{y} = |P_{56}| = 1, \quad b_{12}^{int} = 0, \quad b_{23}^{int} = 0, \quad b_{34}^{int} = 0,$$

$$b_{35}^{int} = |P_{36}| = 2, \quad b_{46}^{int} = |P_{45}| = 2,$$

$$b_{56}^{int} = |P_{36}| + |P_{45}| = 4.$$

466 Note that the maximum interlayer traffic load on this network is fairly low and due

to our choice of paths is $b_{56}^{int} = 4$ although it could have also been minimized to zero, provided that all paths to node 6 bypass edge 56.

At the same time, the interlayer traffic load in the network of Fig. 1(c) is significantly higher since there are no alternatives to go around the "bottle neck" edge 2-3 when traveling from nodes 1 and 2 to nodes 4,5, and 6. For the same choice of shortest paths, we get $b_{23}^{int}=19$. The remaining b_k^x , b_k^y for the network of Fig. 1(c) can be calculated similarly to (5.1). Step 3: Determine α_x^k and α_y^k .

474

467

468

469

470

471

472

473

479

482

483 484

485

486

487 488

The auxiliary systems (4.10) and (4.11) which play the role of a master stability 475 function for synchronization in two-layer networks of Lorenz systems (3.1) take the 476 477

$$\dot{\xi} = \sigma(\eta - \xi) - (a_x + \alpha_x^k)\xi,
\dot{\eta} = (r - z(t))\xi - \eta - x(t)\zeta + \beta\omega_y b_k^{int}\eta
\dot{\zeta} = y(t)\xi + x(t)\eta - b\zeta,$$

$$\begin{split} \dot{\xi} &= \sigma(\eta - \xi) + \beta \omega_x b_k^{int} \xi \\ \dot{\eta} &= (r - z(t)) \, \xi - \eta - x(t) \zeta - (a_y + \alpha_y^k) \eta, \\ \dot{\zeta} &= y(t) \xi + x(t) \eta - b \zeta, \end{split}$$
480 (5.3)

where x(t), y(t), and z(t) correspond to the synchronous solution and are defined by the uncoupled Lorenz system.

As in the auxiliary systems (4.10) and (4.11), the subscripts k in ξ , η , and ζ are omitted to indicate that the 3D auxiliary systems (5.2) and (5.3) should be calculated only once and the desired values of α_x^k and α_y^k for an edge k can simply be read off from the stability diagrams (see Fig. 3). Notice that if the edge is loaded with a high b_k^{int} , then the contribution of the positive term $+\beta\omega_y b_k^{int}\eta$ in the η -equation of system (5.2) cannot always be compensated by increasing $-\alpha_k^k\xi$ in the ξ -equation. Typically, this happens when the positive term exceeds the proper negative linear terms such as $-\eta$ (technically, through a combination of terms in the Routh-Hurwitz criterion).

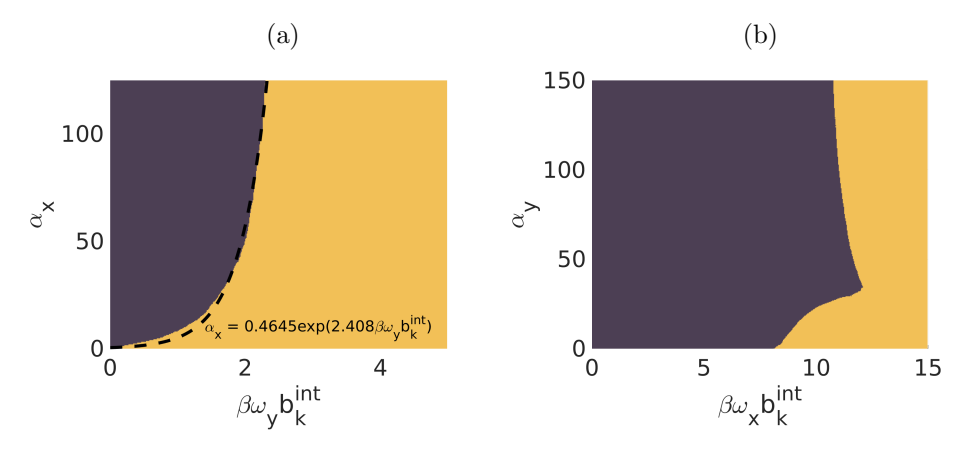


Fig. 3. Stability of the auxiliary systems (5.2) and (5.3) for coupled Lorenz oscillators. Yellow depicts instability of the origin while purple indicates its stability. The dependence of the stabilizing term α_x on $\beta \omega_y b_i^{int}$ is estimated by the exponential function $\alpha_x = 0.4645 \exp{(2.408\beta \omega_y b_i^{int})}$ (dashed curve), and is used to predict synchronization thresholds in networks of Fig. 1 and Fig. 4.

The complex relationship between these terms in regard to stabilizing (5.2) and (5.3) is shown in Fig. 3. Notice the coefficient β on the $\beta \omega_y b_k^{int}$ and $\beta \omega_x b_k^{int}$ axes. The diagrams of Fig. 3 confirm the existence of threshold values for $\beta \omega_y b_k^{int}$ and $\beta \omega_x b_k^{int}$ such that even infinitely large values of α_x and α^y cannot compensate for the caused instability and stabilize systems (5.2) and (5.3).

To better quantify this dependence to be used in predicting synchronization thresholds in networks of Lorenz oscillators, we approximate the stability boundary in Fig. 3(a) by the exponential function

(5.4)
$$\alpha_x = 0.4645 \exp(2.408\beta \omega_u b_k^{int}).$$

The stability diagrams of Fig. 3 along with Fig. 2 account for the role of the individual oscillators composing the networks and the way these oscillators are coupled (through x and y coupling) in the stability of synchronization. These diagrams represent an analog of the master stability function in single-layer networks [49] and help in solving, once and for all, the question of stability for synchronization in two-layer networks involving the Lorenz oscillator through the criterion (4.12), where the role of multilayer network topologies is assessed via the calculation of pure graph theoretical quantities as shown in the next step.

Step 4: Putting pieces together to solve the puzzle. Given the stability diagram of Fig. 3 with abrupt threshold dependences of α_x^k and α_y^k on increasing interlayer traffic load b_k^{int} , the effect of synchrony breaking when a highly loaded x edge is replaced with a better pairwise stabilizing y (see Sec. 3) is no longer a puzzle and directly follows from the application of our stability method. Actually, in a historical retrospective, we first developed the general method that revealed this and other highly counterintuitive effects due to the multilayer structure and then constructed the network examples. To make the presentation more appealing before it becomes too technical, we have decided to put forward the motivating example. As our exhaustive study of various network configurations suggests, we hypothesize that six-node networks of Fig. 1 are minimum size networks of Lorenz oscillators that exhibit the synchrony breaking phenomenon.

To test the predictive power of our approach with the constants identified in Steps 1-3, we perform a systematic study of how one edge replacement, in which we replace only one x edge in the single-layer, x-coupled network of Fig. 1(a) with a y edge, affects synchronization. The edge replacement is performed in the order of the increasing interlayer traffic load on this edge, b_k^{int} . After computing the coupling threshold required to synchronize the new network, this edge reverts back to being an x edge. This results in multiple networks of five x edges and one y edge. The two multilayer networks of Fig. 1(b) and Fig. 1(c) with the drastically different synchronization properties are two instances of this replacement process. Fig. 1(d) presents the actual synchronization threshold values (blue solid line), the interlayer traffic loads b^{int} (black line) calculated similarly to (5.1), and the threshold values predicted by the numerically-assisted criterion (4.4) with constants $a_x = 7.20$, $a_y = 2.63$, $\omega_x = 5.00$ and $\omega_y = 0.50$ chosen above. The constants α_x^k and α_y^k are taken from the diagrams of Fig. 3(a) and Fig. 3(b), respectively. As the stability system (5.2) is much more sensitive to the changes in b_k^{int} than (5.3) (cf. the onset of instability in Figs. 3(a-b)), the threshold values for c_{ij} in the criterion (4.12) for the x layer largely dominate over d_{ij} . Thus, since the synchronization threshold for the entire network (3.1) with uniform coupling c = d is defined by the maximum of the thresholds c_{ij} or d_{ij} for

each edge of the multilayer graph, the maximum threshold values predicted by the 539 540 method and depicted in Fig. 1(d) are the ones corresponding to x edges with coupling c. These threshold values are calculated using (4.12) as follows

$$c > \max_{k} \left\{ c_k = \frac{1}{n} \left[\gamma a_x \cdot b_k^x + \beta \omega_x \cdot b_k^{int} + \alpha_x^k \right] \right\},$$

541

543

544

546

547

548

549

550

552

554

556

558

559

560

561

562

565

566 567

568

569

570

573

574

576

577

578

579

580

581

582

583

584

where α_x^k is defined by the stability diagram of Fig. 3(a) via the approximating function (5.4) for each edge k, and a_x , ω_x , and b_k^{int} are determined in Steps 1-3. The scaling factor γ which is chosen to scale down the term $\frac{a_x}{n}$ to match the coupling needed to synchronize the six-node network of Fig. 1(a) with only x edges. The scaling factor β is then chosen for the network of Fig. 1(b) with the lowest $b_k^{int} = 4$ to match the actual synchronization threshold and then kept constant for predicting the thresholds in the other six-node networks with one replaced x edge. Figure 1(d) shows that the predicted thresholds are fairly close to the actual ones, and the criterion (5.5) correctly predicts an increase or decrease of the coupling threshold for each six-node network and ultimately predicts synchrony break for the network with the replaced x edge 2-3.

As Fig. 1(d) indicates that when lightly loaded edges (edges with fewer chosen paths passing through them) are replaced, the effect on the synchronization stability is fairly small. As discussed in the description of the motivating example, the replacement of x edge 5-6 with a y edge improves synchronization by slightly lowering the synchronization threshold. According to our stability criterion (4.4), this happens due to a slight decrease in the traffic load on the bottleneck edge b_{23}^x (see (5.1)), compared to the original network of Fig. 1(a) with all x edges where one additional path P_{16} goes through edge 2-3. As a result, it decreases the contribution of the dominating term $a_x b_k^x$ in (4.4). At the same time, the contribution of the other factors $\omega_y b_k^{int}$ and α_x^k remain insignificant, especially due to the fact that α_x^k still lies on a flat part of the approximating curve (5.4) before this exponential curve takes off at larger values of b_k^{int} . On the other hand, such a replacement of the bottleneck node 2-3 in the network of Fig. 1(c) significantly increases the intralayer traffic load b_k^{int} , requiring infinitely large α_{23}^x to stabilize the stability system (5.2) and causing synchronization to break.

- 6. Synchrony breakdown in larger networks. To demonstrate that similar synchrony breakdown phenomena occur in larger networks and can be effectively predicted by our method, we consider a 20-node network of Lorenz (and then doublescroll) oscillators described in Fig. 4(a). The network is initially coupled entirely through the x variable. To test our prediction that replacing edges with a high traffic load can make the network unsynchronizable, we index the edges according to their b_{ν}^{x} . Edges similar to edge 10-12 have very few paths that pass through them, and subsequently have a low b_k^x (and in turn, b_k^{int} , shown as the black curve in Fig. 4(c)). We successively replace x edges (denoted by black edges in Fig. 4(a)) with y edges (denoted by gray edges in Fig. 4(b)), according to this ordering until the network is completely connected through y edges. The values of b_k^{int} range from 0 (for edge 10-12 with edge ranking index 1 (see Fig. 4(c)), bypassed by all chosen interlayer paths) to 100 – 400 for highly loaded edges (for example, for edge 3-5 for which every path from node 3 of the x layer graph to any other node in the y-layer must pass through it).
- **6.1.** Twenty-node networks of Lorenz oscillators. The coupling necessary to synchronize the x-coupled Lorenz network (3.1) described in Fig. 4(a) is $c \approx 86.95$. As outlying, low traffic edges are replaced with y edges, there is almost no effect on the

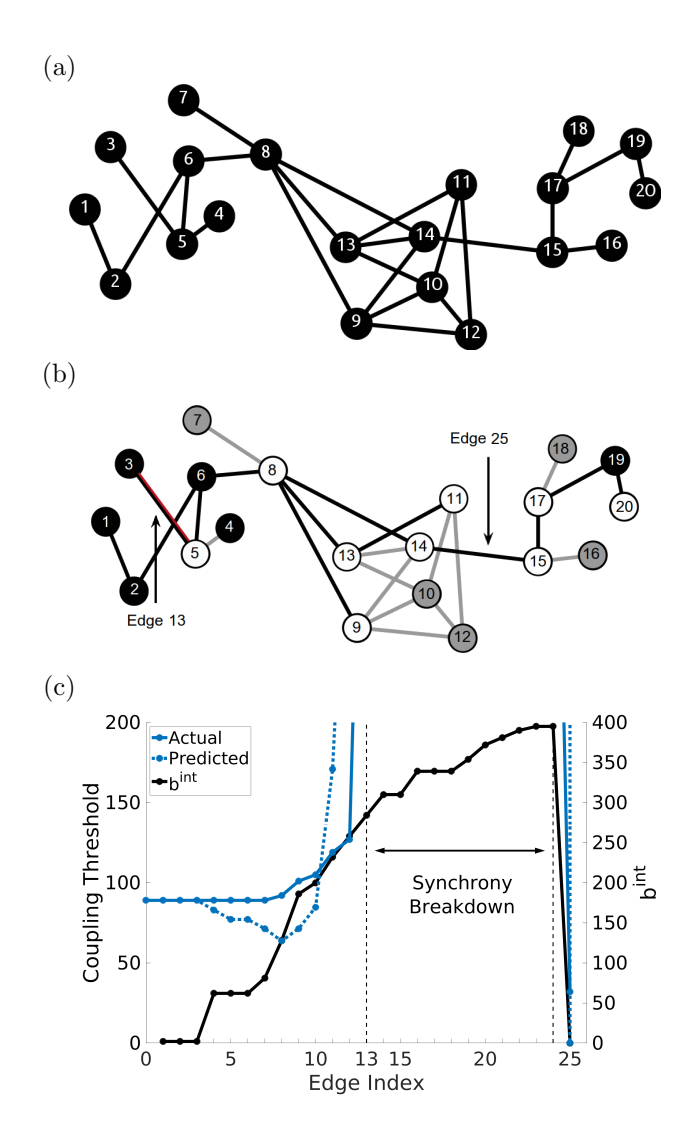


FIG. 4. Effect of successively replacing x coupling edges with y coupling edges on synchronization in a 20-node network of Lorenz oscillators (3.1). (a) Original x-coupled network before replacing edges according to their traffic load. (b) Snapshot of the multilayer network before the edge 3-5, labeled as the 13-th edge according to the traffic load ranking, is replaced. The replacement of this critical edge (red) yields the breakdown of synchronization in the network. Further successive replacement of remaining x edges (gray) with higher traffic load preserves the instability of synchronization, until all 25 edges have been replaced with a y edge, yielding a single-layer y-coupled network with $b^{int}=0$ that is able to synchronize again. (c) Actual (blue solid line) and predicted (blue dotted line) threshold for the coupling strength required to synchronize the network after the i-th x edge has been successively replaced with a y edge. The black solid line depicts the interlayer traffic b^{int} for the respective edge. The predicted coupling thresholds are computed from (5.5) using the exponential fit in Fig. 3 and scaling factors $\beta=0.031$ and $\gamma=0.5993$.

threshold for the coupling strength required to synchronize the network, evidenced by the lack of change in the actual coupling threshold for the first eight edges replaced in Fig. 4(c). As successively more loaded edges are replaced in the network (indicated by the dramatic increase in b^{int}), the network becomes more difficult to synchronize, until edge 13 (edge 3-5 which is depicted in red in Fig. 4(b)) is replaced. After

which, synchronization is no longer feasible for the network for any additional edge replacement, until edge 25 (edge 14-15 in Fig. 4). Replacing edge 25, shown in Fig. 4(b) corresponds to finishing the successive edge replacement process, and results in a graph identical to the one in Fig. 4(a), but in which all of the edges represent y coupling (gray) instead of x coupling (black). This reinforces our traffic load predictions for the breakdown of synchrony in two ways: (i) after enough highly loaded edges are replaced (even with a normally favorable coupling type), the network can no longer synchronize for any coupling strength, (ii) replacing only one edge that is very highly loaded can make the network unsynchronizable, evidenced by the network having no synchronizing coupling value even when all but one edge has been replaced (see edge index 24 in Fig. 4(c)).

As in the six-node example of Fig. 1(a), we have obtained a good fit in Fig. 4(c) which only focuses on placing the stability conditions on x edges in (4.4), because the stability term α_x required to stabilize the x stability system (5.2) must be significantly higher than α_y in the y stability system (5.2) (compare Figs. 3(a-b)). We use the same criterion (5.5) with the same constants a_x , ω_x , and α_x^k to predict the synchronization threshold and only need to identify the traffic loads b_k^{int} and the scaling factors γ and β for a better fit, once and for all variations of the multilayer network topologies used in Fig. 4(c). In contrast to the six-node network example where traffic load b_k^{int} can be easily calculated by hand as in (5.1), computing b_k^{int} for the 20-node or larger networks is a laborious task which was performed by an algebraic algorithm, implemented as MATLAB code and given in the Supplement. While the values of b_k^{int} heavily depend on the choice of paths from one node to another, our algorithm uses the natural choice of the shortest paths, computed via Dijkstra's algorithm [28]. Optimizing the choices of not necessarily shortest paths that distribute traffic loads on edges more equally may yield even better predictions and fits.

6.2. Networks of double scroll oscillators. To illustrate the generality of synchrony break phenomenon when "good" but highly-loaded links go "bad", we apply our numerically-assisted method to networks (2.1), comprised by chaotic double-scroll oscillators [42]

620 (6.1)
$$\dot{x}_{i} = \kappa(y_{i} - x_{i} - h(x)) + \sum_{j=1}^{n} c_{ij}x_{j},$$

$$\dot{y}_{i} = x_{i} - y_{i} + z_{i} + \sum_{j=1}^{n} d_{ij}y_{j},$$

$$\dot{z}_{i} = -\lambda y_{i} - \mu z_{i}, \quad i = 1, ..., n,$$

621 with

622
$$h(x) = \begin{cases} m_1(x+1) - m_0 & x < -1 \\ m_0 x & -1 \le x \le 1 \\ m_1(x-1) + m_0 & x > 1 \end{cases}$$

and standard parameters $\kappa = 10$, $m_0 = -1.27$, $m_1 = -0.68$, $\lambda = 15$, and $\mu = 0.038$.

Similarly to networks of Lorenz oscillators (3.1), a pair of double-scroll oscillators (6.1) can be synchronized through either the x or y variable, and the minimum coupling strength required for synchronization in a two-node y-coupled network, $d^* = 1.16$ is much lower than the coupling threshold in the two-node x-coupled network, $c^* = 5.94$.

In Fig. 5, we apply our method to predict the synchronization thresholds in the 20-node network of Fig. 4 as in the same network of Lorenz oscillators. When successively

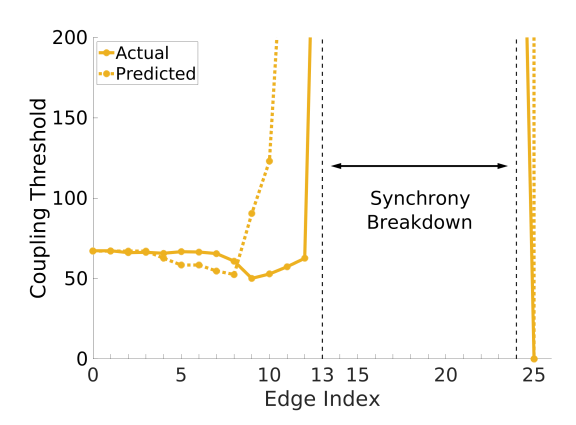


FIG. 5. Effect of successively replacing x edges with y edges on the synchronization threshold in a 20 node network of double-scroll oscillators. The network topology, edge replacement process, and notations are identical to those in Fig. 4(a-b). Notice the same location of critical links (edges 13 to 24) whose replacement leads to synchrony breaks as in the network of Lorenz oscillators (cf. Fig. 4(c)).

 replacing x edges in the network, there is initially a decrease in the coupling threshold for synchronization, when peripheral edges or edges in highly connected regions of the graph with low traffic loads b_k^{int} are replaced with more favorable y edges that provide better pairwise convergence to synchronization. Then, as with the network of Lorenz oscillators, when edge 13 (edge 3-5) is replaced with a y edge, synchronization is no longer attainable. Synchronization then returns when the entire x-coupled network has been replaced with y edges. Notably, the synchrony break occurs at the same edge as in the network of Lorenz oscillators, suggesting that critical edges whose replacement hampers synchronization are mainly controlled by the network multilayer topology rather than the individual properties of the intrinsic oscillators, provided that the oscillators possess similar synchronization properties as the Lorenz and double scroll oscillators.

The solid curve in Fig. 5 displays the synchronization thresholds, calculated via the stability criterion (5.5) with $a_x = 5.94 \times 2 = 11.88$, $\omega_y = 1.0$, $\beta = 0.0095$, $\gamma = 0.282$, and the approximating function $\alpha_x = 1.556 \exp(3.711\beta\omega_y b_k^{int})$ with the same traffic loads b_k^{int} shown in Fig. 4. This approximating function is obtained from a stability diagram for coupled double scroll-oscillators which is computed similarly to Fig. 3 and displays a similar threshold effect as in Fig. 3 [not shown]. As in the Lorenz oscillator case, the auxiliary stability system (4.5) for α_x is much more sensitive to increasing b_k^{int} than the stability system (4.6) for α_y , therefore one can only evaluate the stability condition (5.5) for the x coupling x to identify a bottle-neck for the synchronization threshold in the entire network.

Going back to the puzzle example, we have also performed a similar analysis of the six-node network of Fig. 1 where the Lorenz oscillators are replaced with the double-scroll oscillators [not shown]. Remarkably, this analysis indicates the same qualitative phenomena when the replacement of the lightly loaded edge 5-6 slightly lowers the synchronization threshold from c=13.57 in the original x-coupled single-layer network of Fig. 1(a) to c=13.36, and predicts the breakdown of synchrony when edge 2-3 is replaced as in the Lorenz network.

We have also simulated series of other 20-node networks (3.1) and then networks (6.1) where *all* oscillators were connected via x layer graphs, whereas the y coupling

only connected some of the oscillators. In contrast to the networks of Fig. 1 and Fig. 4 where the critical highly-loaded links separate the network into disjoint x and y graph components, these networks do not show the effect of synchrony breaking as any pair of nodes is coupled directly or indirectly via the x graph such that the coupling strengths c can be made strong enough to stabilize synchronization. However, the synchronization thresholds in such networks depend on the location of added y edges in a nonlinear fashion. In support of this claim, we draw the reader's attention to the six-node example of Fig. 1(b) where the x graph connects all six nodes and the replacement of edge 5-6 with an y edge lowers the synchronization threshold. On the contrary, the replacement of the x edge 3-5 with an edge y, which still preserves the connectedness of the x graph, increases the synchronization threshold, as predicted by the method (see Fig. 1(c)). The 20-node networks with connected x graphs yield similar effects. To avoid repetition, these results are not shown.

6.3. Networks of Hindmarsh-Rose oscillators. To convince the reader that the counterintuitive effects of synchrony breaking do not originate from the chaoticity of the oscillators, we have considered a network of limit-cycle Hindmarsh-Rose oscillators [7]:

679 (6.2)
$$\dot{x}_{i} = ax_{i}^{2} - y_{i} - z_{i} + \sum_{j=1}^{n} c_{ij}x_{j},$$

$$\dot{y}_{i} = (a + \alpha)x_{i} - y_{i} + \sum_{j=1}^{n} d_{ij}y_{j},$$

$$\dot{z}_{i} = \mu(bx_{i} + c - z_{i}), \quad i = 1, ..., n.$$

 The individual Hindmarsh-Rose model represents a class of spiking and bursting neurons where x describes the membrane potential, and the variables y and z take into account the transport of ions across the membrane through fast and slow ion channels, respectively. The Hindmarsh-Rose model exhibits periodic square-wave bursting across a wide range of parameters, including the chosen parameters $a=2.8, \alpha=1.6, c=5, b=9, \mu=0.001$ [9].

While coupling through the y variables does not make physiological sense, we use this network as a phenomenological example of a multilayer network of periodic oscillators which exhibits the same effect of synchrony breaking observed in the networks of chaotic Lorenz and double scroll oscillators. The analysis of the six-node network of Fig. 1 where the chaotic Lorenz oscillators are replaced with the perodic Hindmarsh-Rose oscillators yields a similar dependence of the synchronization thresholds as a function of the edge replacement [not shown]. In particular, the threshold coupling for the network of Fig. 1(b) where the lightly loaded x edge 5-6 is replaced with a y edge is c=1.66. However, the replacement of the highly loaded x edge 2-3 (see Fig. 1(c)) yields an infinitely large synchronization threshold as in the examples of the Lorenz and double scroll oscillators. This suggests that the synchronization breakdown effect is not rooted in the particular properties of the chosen limit-cycle or chaotic oscillators but rather defined by the structure of a multilayer network and the location of highly loaded links.

7. Predicting synchrony in large random networks. Our numerically-assisted Multilayer Connection Graph Method is also applicable to large, possibly random networks for which the intralayer and interlayer traffic loads can be calculated similarly to the 20-node networks through the MATLAB algebraic algorithm given in the Supplement. The algebraic algorithm is rooted in the Dijkstra algorithm

and sorting the shortest paths and therefore has a comparable complexity. This complexity along with the required computer power are limitations on the (very large) network size that can be handled by the method. In this regard, predicting synchronization in reasonably large networks of 100-1000 nodes via the stability criterion (5.5) based on the calculations of traffic loads b_k^x , b_k^y , and b_k^{int} is a simple, computationally inexpensive task, comparable to the application of the connection graph method or master stability function to predicting synchronization in single-layer networks.

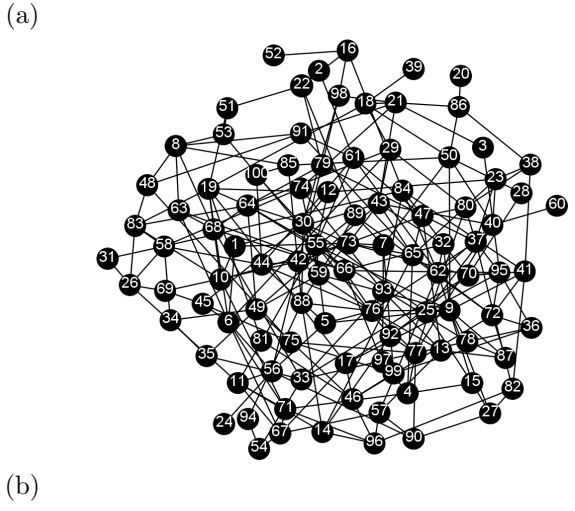
 $705 \\ 706$

722

Figure 6 demonstrates the actual and predicted synchronization thresholds in 100-node two-layer Erdős-Rényi networks of Lorenz oscillators (3.1). The procedure for constructing these two-layer random networks is as follows. We begin with a single-layer x-coupled Erdős-Rényi network whose edges are generated with probability p=0.05. Then, we generate five two-layer networks obtained from the 100 random Erdős-Rényi network by replacing 25% of randomly chosen x edges with y edges. These five networks have the same fraction of x and y edges but the structures of their x and y layers are different (the adjacency lists of their two-layer network topologies are given in the Supplement). Figure 6(b) shows that these highly connected networks do not exhibit the synchronization breakdown effect due to the absence of bottle neck edges that would separate the layers and correspond to high interlayer traffic load b_k^{int} . Indeed, the maximum traffic load b_k^{int} for the most loaded edge in each of the five networks is nearly the same such that the synchronization thresholds do not vary significantly.

8. Conclusions. While the study of synchronization in multilayer dynamical networks has gained significant momentum, the general problem of assessing the stability of synchronization as a function of multilayer network topology remained practically untouched due to the absence of general predictive methods. The existing eigenvalue methods, including the master stability function [49], which effectively predict synchronization thresholds in single-layer networks cannot be applied to multilayer networks in general. This is due to the fact that the connectivity matrices corresponding to two or more connection layers do not commute in general, and therefore, the eigenvalues of the connectivity matrices cannot be used. Therefore, synchronization in multilayer networks is usually studied on a case by case basis either via (i) full-scale simulations of all transversal Lyapunov exponents of the $(n-1) \times s$ -dimensional system of variational equations [27], where n is the network size and s is the dimension of the intrinsic node dynamics, or more effectively via (ii) simultaneous block diagonalization of the connectivity matrices [36] which in some cases can reduce the problem of assessing synchronization in a large network to a smaller network which, however, contains positive and negative connections, including self loops such that the exact role of multilayer network topology and the addition or exchange of edges remains unclear.

In this paper, we have made significant progress in understanding synchronization properties of multilayer networks by developing a predictive method, called the Multilayer Connection Graph method, which does not rely on calculations of eigenvalues of the connectivity matrices, and therefore can handle multilayer networks. Originated from the connection graph method for synchronization in single-layer networks [16], our method combines stability theory with graph theoretical reasoning. Two key ingredients of the method are (i) the calculation of stability diagrams for the auxiliary s-dimensional system which indicate how the dynamics of the given oscillator comprising the network can be stabilized via one variable corresponding to one connection layer when an instability is introduced via the other variable from



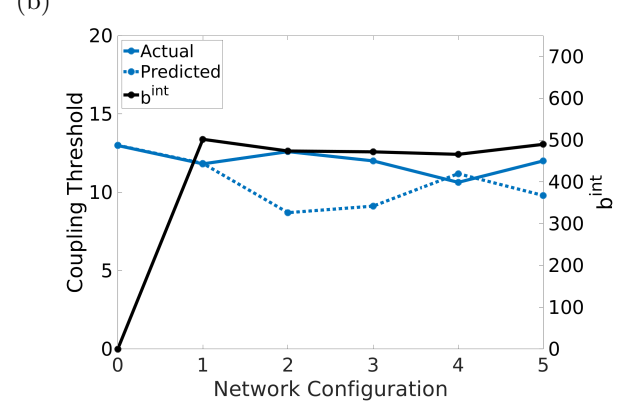


Fig. 6. Synchronization in two-layer random Erdős-Rényi networks of 100 Lorenz oscillators (3.1). (a) Original x-coupled Erdős-Rényi network generated with probability p=0.005 for the presence of an x edge. (b). Actual (blue solid line) and predicted (blue dotted line) synchronization thresholds in five two-layer network configurations obtained from the 100 random Erdős-Rényi network by replacing 25% of randomly chosen x edges with y edges. The black solid line depicts the interlayer traffic b^{int} for an edge with the highest traffic load. Notice only minor changes in b^{int} and, therefore, in the synchronization thresholds in the five two-layer network configurations with the same fraction of x and y edges. Similarly to Fig. 4, the predicted thresholds are computed from (5.5) using the exponential fit in Fig. 3 and scaling factors $\beta=0.012365$ and $\gamma=0.365$.

another connection layer and (ii) the calculation of traffic loads via a given edge on the multilayer connection graph. All together, these quantities allow for predicting the synchronization threshold and identify critical links that control synchronization in the original, potentially large, multilayer network.

Using the method, we have discovered striking, highly unexpected phenomena not seen in single-layer networks. In particular, we have shown that replacing a link with a light interlayer traffic load by a stronger pairwise converging coupling via another layer may improve synchronizability, as one would expect. At the same time, such a replacement of a highly loaded link may essentially worsen synchronizability and make the network unsynchronizable, turning the pairwise stabilizing "good" link into a destabilizing connection (a "bad" link). The critical links whose replacement can lead to synchrony break are typically the ones that connect the layers such the

oscillators from two layers become coupled through the intrinsic, nonlinear equations of the individual oscillator that correspond to a "relay" node passed by the only path from one layer to the other. As a result, the intrinsic dynamics of the individual node oscillator plays a pivotal role in the stability of synchronization. In this paper, we have limited our attention to Type I limit-cycle and chaotic oscillators such as the Lorenz, double scroll, and Hindmarsh-Rose oscillators that yield synchronization that remains stable in a single-layer network once the coupling exceeds a critical threshold. Remarkably, when used in a multilayer network, these oscillators have indicated similar synchronization properties, suggesting that the location of critical edges in the considered network may remain unchanged for other Type I oscillators. While our method for assessing synchronization is only applicable to Type I oscillators, it could be modified to handle Type II networks, including multilayer networks of Rössler systems [49]. This modification is a subject of future study.

To gain insight into the determining factors for the emergence of synchrony breaking, without potential confounds associated with the interplay between multiple layers and direction of links, we have considered examples of two-layer undirected networks of identical oscillators. However, the extension of our general method, which was developed for three-layer networks and applied to two-layer networks in this paper, to multiple layers, directed networks and non-identical oscillators is fairly straightforward and will be reported elsewhere. In particular, the extension of our method to directed networks can be performed by adapting the generalized connection graph method [5, 6] for single-layer directed networks, where directed edges are symmetrized and assigned additional weights according to the mean node unbalance. In the case of slightly non-identical oscillators, perfect synchronization cannot exist, but approximate synchronization in multilayer networks is still possible. Our Multilayer Connection Graph method can be easily extended to such non-identical oscillators by assessing the stability of a δ -neighborhood of the generating synchronization manifold, similarly to the single layer connection graph method (see Appendix B in [16]).

Our method can also be modified to handle multilayer neuronal networks connected via electrical, excitatory, and inhibitory synapses which exhibit a number of counterintuitive synergistic effects: when (i) the addition of pairwise repulsive inhibition to single-layer excitatory networks can promote synchronization [13] and (ii) combined electrical and inhibitory coupling can induce synchronization even though each coupling alone promotes an anti-phase rhythm [55]. Our method promises to allow an analytical treatment of these effects in large neuronal networks which has been impaired by the absence of predictive methods that can handle excitatory, inhibitory, and electrical neuronal circuitries simultaneously. A key to addressing this issue is the construction of auxiliary stability diagrams that incorporate the variational equations for the stability of the synchronous bursting solution in such networks [13, 55] with the traffic loads on critical links. This study will be reported elsewhere.

9. Appendix. In this appendix we derive the Multilayer Connection Graph method and prove Theorem 4.1. Our goal is to derive the conditions of global asymptotic stability of the synchronization manifold S in the system (2.1). To achieve this goal and develop the stability method, we follow the steps of the proof of the connection graph method [16]. The concept is similar, up to a certain step where a new stability argument is used.

In the network model (2.1) we introduce the difference variable

813 (9.1)
$$\mathbf{X}_{ij} = \mathbf{x}_j - \mathbf{x}_i, \ i, j = 1, ..., n,$$
22

whose convergence to zero will imply the transversal stability of the synchronization manifold S.

Subtracting the *i*-th equation from the *j*-th equation in system (2.1), we obtain the equations for the transversal stability of S

(9.2)
$$\dot{\mathbf{X}}_{ij} = \mathbf{F}(\mathbf{x}_j) - \mathbf{F}(\mathbf{x}_i) + \sum_{k=1}^{n} \{c_{jk}P\mathbf{X}_{jk} - c_{ik}P\mathbf{X}_{ik} + d_{jk}L\mathbf{X}_{jk} - d_{ik}L\mathbf{X}_{ik} + g_{jk}M\mathbf{X}_{jk} - g_{ik}M\mathbf{X}_{ik}\}, \quad i, j = 1, ..., n.$$

To obtain the explicit dependence of $\mathbf{F}(\mathbf{x}_j) - \mathbf{F}(\mathbf{x}_i)$ on \mathbf{X}_{ij} , we introduce the following vector notation

$$\mathbf{F}(\mathbf{x}_j) - \mathbf{F}(\mathbf{x}_i) = \left[\int_0^1 D\mathbf{F}(v\mathbf{x}_j + (1-v)\mathbf{x}_i) dv \right] \mathbf{X}_{ij},$$

where $D\mathbf{F}$ is the 3×3 Jacobian matrix of \mathbf{F} . This notation is simply a compact form of the mean value theorem, f(B) - f(A) = f'(C)(B - A), applied to the vector functions $\mathbf{F}(\mathbf{x}_j)$ and $\mathbf{F}(\mathbf{x}_i)$, where the Jacobian $D\mathbf{F}$ is evaluated at some point $C \in [\mathbf{x}_i, \mathbf{x}_j]$.

Therefore, the difference system (9.2) can be rewritten in the form

(9.3)
$$\dot{\mathbf{X}}_{ij} = \begin{bmatrix} \int_{0}^{1} D\mathbf{F}(v\mathbf{x}_{j} + (1-v)\mathbf{x}_{i})dv \end{bmatrix} \mathbf{X}_{ij} + \sum_{k=1}^{n} \{c_{jk}P\mathbf{X}_{jk} - c_{ik}P\mathbf{X}_{ik} + d_{jk}L\mathbf{X}_{jk} - d_{ik}L\mathbf{X}_{ik} + g_{jk}M\mathbf{X}_{jk} - g_{ik}M\mathbf{X}_{ik}\}, \quad i, j = 1, ..., n.$$

The first term in the brackets yields instability via the divergence of trajectories within the individual, possibly chaotic oscillators. The second (summation) term, which represents the contribution of the network connections, may overcome the unstable term, provided that the coupling is strong enough.

Notice that the stability of system (9.3) is redundant as it contains all possible (n-1)n/2 non-zero differences \mathbf{X}_{ij} along with n zero differences $\mathbf{X}_{ii} = 0$ which can be disregarded. At the same time, there are only n-1 linearly independent differences required to show the convergence between n variables \mathbf{X}_{ij} . However, this redundancy property and the consideration of all non-zero \mathbf{X}_{ij} are a key ingredient of our approach which allows for separating the difference variables later in the stability description, without diagonalizing the connectivity matrices.

We strive to find conditions under which the trivial fixed point $\{\mathbf{X}_{ij} = 0, i, j = 1, ..., n\}$ of system (9.3) is globally stable. This amounts to finding conditions for global stability of synchronization in the network (2.1).

We introduce the following terms $A_{ij}\mathbf{X}_{ij}$, where A_{ij} is a 3×3 matrix, such that²

$$A_{ij} = \begin{cases} a_x P &= \operatorname{diag}(a_x, 0, 0) \text{ if oscillators } i \text{ and } j \\ \operatorname{belong to } x \text{ layer } C \\ a_y L &= \operatorname{diag}(0, a_y, 0) \text{ if oscillators } i \text{ and } j \\ \operatorname{belong to } y \text{ layer } D \\ a_z M &= \operatorname{diag}(0, 0, a_z) \text{ if oscillators } i \text{ and } j \\ \operatorname{belong to } z \text{ layer } G \\ K &= \operatorname{diag}(\omega_x, \omega_y, \omega_z) \text{ if oscillators } i \text{ and } j \\ \operatorname{belong to } different \text{ layers,} \end{cases}$$

where constants $a_x, a_y, a_z, \omega_x, \omega_y, \omega_z$ are to be determined.

838

854

855 856

857

We add and subtract additional terms $A_{ij}\mathbf{X}_{ij}$ with matrix A_{ij} defined in (9.4) from the stability system (9.3) and obtain (9.5)

$$\dot{\mathbf{X}}_{ij} = \begin{bmatrix} \int_{0}^{1} D\mathbf{F}(v\mathbf{x}_{j} + (1-v)\mathbf{x}_{i})dv - A_{ij} \end{bmatrix} \mathbf{X}_{ij} + A_{ij}\mathbf{X}_{ij} + \sum_{k=1}^{n} \{c_{jk}P\mathbf{X}_{jk} - c_{ik}P\mathbf{X}_{ik} + d_{jk}L\mathbf{X}_{jk} - d_{ik}L\mathbf{X}_{ik} + g_{jk}M\mathbf{X}_{jk} - g_{ik}M\mathbf{X}_{ik} \}.$$

The introduction of the terms $A_{ij}\mathbf{X}_{ij}$ allows for obtaining stability conditions of the trivial fixed point $\mathbf{X}_{ij} = 0$, i, j = 1, ..., n in two steps. Note that the matrix $-A_{ij}$ 845 contributes to the stability of the fixed point and can compensate for instabilities induced by eigenvalues with nonnegative real parts of the Jacobian DF. This can be 847 achieved by increasing parameters $a_x, a_y, a_z, \omega_x, \omega_y$, and ω_z . At the same time, the 848 instability originated from its positively definite counterpart, matrix $+A_{ij}$, can be 849 damped by the coupling terms through c_{ij} , d_{ij} , and g_{ij} . 850 Step I. We make the first step by introducing the following auxiliary systems for 851 852 i, j = 1, ..., n

853 (9.6)
$$\dot{\mathbf{X}}_{ij} = \left[\int_{0}^{1} D\mathbf{F}(v\mathbf{x}_j + (1-v)\mathbf{x}_i) \, dv - A_{ij} \right] \mathbf{X}_{ij}.$$

This system is identical to system (9.5) where the coupling terms are removed.

 A_{ij} can take four different forms, depending on whether oscillators i and j both belong to the x or y or z graphs, or belong to different graphs, for example, if i belongs to the x graph, and j belongs to the y graph (see (9.4)). Therefore, we have four types

 $^{^2}$ A different choice of matrix K which takes the values: (i) $\operatorname{diag}(\omega_x, \omega_y, 0)$ if the path between oscillators i and j is only composed of x and y edges, (ii) $\operatorname{diag}(0, \omega_y, \omega_z)$ if the path between oscillators i and j is only composed of y and z edges, (iii) $\operatorname{diag}(\omega_x, 0, \omega_z)$ if the path between oscillators i and j is only composed of x and z edges, and (iv) $\operatorname{diag}(\omega_x, \omega_y, \omega_z)$ if the path between oscillators i and j contains x, y, and z edges, may yield lower bounds on the coupling thresholds c_k , d_k , and g_k in the stability criterion (9.31). This is due to the fact that splitting the matrix K into the four matrices may lower the interlayer traffic load on edge k, b_k^{int} . However, this makes practical applications of the method less convenient as the more conservative bounds on b_k^{int} can be balanced out by the choice of the scaling parameter β . Furthermore, one would have to impose additional constraints on ω_x , ω_y , and ω_z that must be large enough to guarantee that every pair (ω_x, ω_y) , (ω_y, ω_z) , and (ω_x, ω_z) must yield global synchronization in the corresponding two-node network, as opposed to lower values guaranteed by the triple $(\omega_x, \omega_y, \omega_z)$ used in the matrix K in (9.4).

858 of the auxiliary systems

(9.7)
$$\dot{\mathbf{X}}_{ij} = \begin{bmatrix} \int_{0}^{1} D\mathbf{F}(v\mathbf{x}_{j} + (1-v)\mathbf{x}_{i}) \ dv - a_{x}P \end{bmatrix} \mathbf{X}_{ij}$$
 if i and j both belong to x layer,

(9.8)
$$\dot{\mathbf{X}}_{ij} = \begin{bmatrix} \int_{0}^{1} D\mathbf{F}(v\mathbf{x}_{j} + (1-v)\mathbf{x}_{i}) \ dv - a_{y}L \end{bmatrix} \mathbf{X}_{ij}$$
 if i and j both belong to y layer,

(9.9)
$$\dot{\mathbf{X}}_{ij} = \begin{bmatrix} \int_{0}^{1} D\mathbf{F}(v\mathbf{x}_{j} + (1-v)\mathbf{x}_{i}) dv - a_{z}M \end{bmatrix} \mathbf{X}_{ij}$$
 if i and j both belong to z layer,

(9.10)
$$\dot{\mathbf{X}}_{ij} = \begin{bmatrix} \int_{0}^{1} D\mathbf{F}(v\mathbf{x}_{j} + (1-v)\mathbf{x}_{i}) \ dv - K \end{bmatrix} \mathbf{X}_{ij}$$
 if i and j belong to different layers.

Remarkably, the auxiliary system (9.7) coincides with the difference system for the global stability of synchronization in a two-oscillator network (2.1) with only x coupling, where a_x plays the role of the double coupling strength that guarantees the stability (see [16] for a detailed discussion on this relation).

Similarly, the stability of auxiliary system (9.8) [(9.9)] implies global stability of synchronization in the two-node network (2.1) with only y(z) coupling, where $a_y(a_z)$ is the double coupling strength of the y(z) connection. Lastly, the stability of auxiliary system (9.10) guarantees globally stable synchronization in the two-node network with all x, y, and z coupling, where a combination of constants ω_x, ω_y , and ω_z , present in K, is a combination of the double coupling strengths of x, y and z connections that is sufficient to induce stable synchronization in the xyz-coupled two-node network.

Therefore, our immediate goal is to find upper bounds on the values of a_x , a_y , a_z , ω_x , ω_y , and ω_z that make the origin of the auxiliary systems (9.7)-(9.10) stable. This amounts to proving global synchronization in the four x-, y-, z-, and xyz-coupled networks that are composed of two oscillators. As only Type I oscillators [21] are capable of synchronizing globally and retaining synchronization for any coupling strength exceeding some critical threshold, our approach based on the calculation of a_x , a_y , and a_z is thus limited to this class of oscillators.

The proof of global stability in (9.7)-(9.10) and derivation of bounds a_x , a_y , a_z and ω_x , ω_y , ω_z involves the construction of a Lyapunov function along with the assumption of the eventual dissipativeness of the coupled system. Therefore, before advancing with the study of larger networks (2.1), one has to prove that globally stable synchronization in the simplest x-, y-, z-, and xyz-coupled two-oscillator networks is achievable. The bound a_x for x-coupled Lorenz oscillators was given in [16]. Upper bounds for a_y , a_z , ω_x , ω_y , ω_z can be derived similarly.

Having obtained the bounds a_x , a_y , a_z , and ω_x , ω_y , ω_z , and therefore proving the stability of the auxiliary systems (9.7)- (9.10), we can take the second step in analyzing the full stability system (9.5).

Step II. The bounds a_x , a_y , a_z and ω_x , ω_y , ω_z that stabilize the auxiliary systems (9.7)-(9.10) reduce the stability analysis of system (9.5) to the following equations by excluding the term in brackets

$$\begin{array}{rcl}
\mathbf{\dot{X}}_{ij} &=& A_{ij}\mathbf{X}_{ij} + \sum_{k=1}^{n} \{c_{jk}P\mathbf{X}_{jk} - c_{ik}P\mathbf{X}_{ik} + d_{jk}L\mathbf{X}_{jk} - d_{ik}L\mathbf{X}_{ik} + g_{jk}M\mathbf{X}_{jk} - g_{ik}M\mathbf{X}_{ik}\}, \ i, j = 1, ..., n.
\end{array}$$

- Note that the positive term $A_{ij}\mathbf{X}_{ij}$, which contains the upper bounds a_x , a_y , a_z and $\omega_x, \omega_y, \omega_z$, is destabilizing and must be compensated for by the coupling terms. To
- study the stability of (9.11) we introduce a Lyapunov function of the form

902 (9.12)
$$V = \frac{1}{4} \sum_{i=1}^{n} \sum_{j=1}^{n} \mathbf{X}_{ij}^{T} \cdot I \cdot \mathbf{X}_{ij},$$

- 903 where I is a 3×3 identity matrix.
- Its time derivative with respect to system (9.11) becomes

$$\dot{V} = \frac{1}{2} \sum_{i=1}^{n} \sum_{j=1}^{n} \mathbf{X}_{ij}^{T} A_{ij} \mathbf{X}_{ij} - \frac{1}{2} \sum_{i=1}^{n} \sum_{j=1}^{n} \sum_{k=1}^{n} \{c_{jk} \mathbf{X}_{ji}^{T} P \mathbf{X}_{jk} + c_{ik} \mathbf{X}_{ik}^{T} P \mathbf{X}_{ij}\} - \frac{1}{2} \sum_{i=1}^{n} \sum_{j=1}^{n} \sum_{k=1}^{n} \{d_{jk} \mathbf{X}_{ji}^{T} L \mathbf{X}_{jk} + d_{ik} \mathbf{X}_{ik}^{T} L \mathbf{X}_{ij}\} - \frac{1}{2} \sum_{i=1}^{n} \sum_{j=1}^{n} \sum_{k=1}^{n} \{g_{jk} \mathbf{X}_{ji}^{T} M \mathbf{X}_{jk} + g_{ik} \mathbf{X}_{ik}^{T} M \mathbf{X}_{ij}\}.$$

We need to demonstrate the negative semi-definiteness of the quadratic form \dot{V} .

As $(\mathbf{X}_{ii}^2 = 0, \mathbf{X}_{ij}^2 = \mathbf{X}_{ji}^2)$, the first sum simplifies to

908 (9.14)
$$S_1 = \sum_{i=1}^{n-1} \sum_{i>i}^n A_{ij} \mathbf{X}_{ij}^2.$$

This sum is always positive definite and its contribution must be compensated for by the second, third, and fourth sums

$$S_{2} = -\frac{1}{2} \sum_{i=1}^{n} \sum_{j=1}^{n} \sum_{k=1}^{n} \{c_{jk} \mathbf{X}_{ji}^{T} P \mathbf{X}_{jk} + c_{ik} \mathbf{X}_{ik}^{T} P \mathbf{X}_{ij}\},$$

$$S_{3} = -\frac{1}{2} \sum_{i=1}^{n} \sum_{j=1}^{n} \sum_{k=1}^{n} \{d_{jk} \mathbf{X}_{ji}^{T} L \mathbf{X}_{jk} + d_{ik} \mathbf{X}_{ik}^{T} L \mathbf{X}_{ij}\}$$

$$S_{4} = -\frac{1}{2} \sum_{i=1}^{n} \sum_{j=1}^{n} \sum_{k=1}^{n} \{g_{jk} \mathbf{X}_{ji}^{T} M \mathbf{X}_{jk} + g_{ik} \mathbf{X}_{ik}^{T} M \mathbf{X}_{ij}\}.$$

Due to the coupling symmetry, the two terms in S_2 , S_3 , and S_4 can be made identical by exchanging the indices i with j in the second terms such that

$$S_{2} = -\sum_{i=1}^{n} \sum_{j=1}^{n} \sum_{k=1}^{n} c_{jk} \mathbf{X}_{ji}^{T} P \mathbf{X}_{jk},$$

$$S_{3} = -\sum_{i=1}^{n} \sum_{j=1}^{n} \sum_{k=1}^{n} d_{jk} \mathbf{X}_{ji}^{T} L \mathbf{X}_{jk},$$

$$S_{4} = -\sum_{i=1}^{n} \sum_{j=1}^{n} \sum_{k=1}^{n} g_{jk} \mathbf{X}_{ji}^{T} M \mathbf{X}_{jk}.$$

Taking into account that $\mathbf{X}_{jj} = 0$, we obtain

$$S_{2} = -\sum_{i=1}^{n} \sum_{k=1}^{n-1} \sum_{j>k}^{n} c_{jk} \mathbf{X}_{ji}^{T} P \mathbf{X}_{jk} - \sum_{i=1}^{n} \sum_{k=1}^{n-1} \sum_{j

$$S_{3} = -\sum_{i=1}^{n} \sum_{k=1}^{n-1} \sum_{j>k}^{n} d_{jk} \mathbf{X}_{ji}^{T} L \mathbf{X}_{jk} - \sum_{i=1}^{n} \sum_{k=1}^{n-1} \sum_{j

$$S_{4} = -\sum_{i=1}^{n} \sum_{k=1}^{n-1} \sum_{j>k}^{n} g_{jk} \mathbf{X}_{ji}^{T} M \mathbf{X}_{jk} - \sum_{i=1}^{n} \sum_{k=1}^{n-1} \sum_{j$$$$$$

Again, exchanging j and k in the second terms of S_2 , S_3 and S_4 and implying the symmetries of coupling $c_{jk} = c_{kj}$, $d_{jk} = d_{kj}$, and $g_{jk} = g_{kj}$, we obtain

$$S_{2} = -\sum_{i=1}^{n} \sum_{k=1}^{n-1} \sum_{j>k}^{n} c_{jk} (\mathbf{X}_{ji}^{T} + \mathbf{X}_{ik}^{T}) P \mathbf{X}_{jk},$$

$$S_{3} = -\sum_{i=1}^{n} \sum_{k=1}^{n-1} \sum_{j>k}^{n} d_{jk} (\mathbf{X}_{ji}^{T} + \mathbf{X}_{ik}^{T}) L \mathbf{X}_{jk},$$

$$S_{4} = -\sum_{i=1}^{n} \sum_{k=1}^{n-1} \sum_{j>k}^{n} g_{jk} (\mathbf{X}_{ji}^{T} + \mathbf{X}_{ik}^{T}) M \mathbf{X}_{jk}.$$

920 Since
$$\mathbf{X}_{ji}^T + \mathbf{X}_{ik}^T = \left[\mathbf{x}_i^T - \mathbf{x}_j^T + \mathbf{x}_k^T - \mathbf{x}_i^T\right] = \mathbf{X}_{jk}^T$$
, we obtain

$$S_{2} = -\sum_{k=1}^{n-1} \sum_{j>k}^{n} n c_{jk} \mathbf{X}_{jk}^{T} P \mathbf{X}_{jk},$$

$$S_{3} = -\sum_{k=1}^{n-1} \sum_{j>k}^{n} n d_{jk} \mathbf{X}_{jk}^{T} L \mathbf{X}_{jk},$$

$$S_{4} = -\sum_{k=1}^{n-1} \sum_{j>k}^{n} n g_{jk} \mathbf{X}_{jk}^{T} M \mathbf{X}_{jk}.$$

Returning to the derivation of the Lyapunov function (9.13) and combining the sums S_1, S_2, S_3, S_4 yields the condition which guarantees that $\dot{V} \leq 0$:

924 (9.20)
$$S_1 + S_2 + S_3 + S_4 = \sum_{i=1}^{n-1} \sum_{j>i}^n \mathbf{X}_{ij}^T [A_{ij} - nc_{ij}P - nd_{ij}L - ng_{ij}M] \mathbf{X}_{ij} < 0.$$

The most remarkable property of this condition is that we are able to eliminate the cross terms and formulate the condition in terms of \mathbf{X}_{ij} . This is because we chose to consider the redundant system with all possible differences \mathbf{X}_{ij} , including linearly dependent ones.

The condition (9.20) finally transforms into

929

930 (9.21)
$$n \sum_{i=1}^{n-1} \sum_{j>i}^{n} [c_{ij} \mathbf{X}_{ij}^T P \mathbf{X}_{ij} + d_{ij} \mathbf{X}_{ij}^T L \mathbf{X}_{ij} + g_{ij} \mathbf{X}_{ij}^T M \mathbf{X}_{ij}] > \sum_{i=1}^{n-1} \sum_{j>i}^{n} \mathbf{X}_{ij}^T A_{ij} \mathbf{X}_{ij}.$$

931 Notice that the left-hand side (LHS) of this inequality contains only the differences

 \mathbf{X}_{ij} between the oscillators that belong to the edges on the connection graphs C, D,

933 and G: the first term on the LHS corresponds to the x layer, the second term is

934 defined by the edges of the y layer, and the third term corresponds to the z layer. At

the same time, the variables on the right-hand side (RHS) of (9.21) correspond to all

936 possible differences between pairs of oscillators that might or might not be defined by

edges of the connection graphs. Hence, to get rid of the presence of the differences \mathbf{X}_{ij} and therefore find the conditions explicit in the parameters of the network model (2.1), we express the differences on the RHS via the differences on the LHS such that we will be able to cancel them.

So far, we have closely followed the steps in the derivation of the connection graph method [16] for single-layer networks. The inequality (9.21) is similar to that of the connection graph method, except for the presence of the second and third terms on the LHS and a modified matrix A_{ij} . A new non-trivial observation, however, is that the total number of oscillators, n, in the network (2.1), composed of three connectivity layers, appears as a factor in all three sums on the LHS, corresponding to the x, y and z layers, even though each layer itself may contain fewer oscillators. The stability argument which follows drastically differs from that of the connection graph method.

Denote on the LHS of (9.21): (i) the differences \mathbf{X}_{ij} corresponding to edges of the x graph by $\tilde{\mathbf{X}}_k$, k=1,...,m, (ii) the differences \mathbf{X}_{ij} corresponding to edges of the y graph by $\tilde{\mathbf{Y}}_k$, k=1,...,l, and (iii) the differences \mathbf{X}_{ij} corresponding to edges of the z graph by $\tilde{\mathbf{Z}}_k$, k=1,...,q. Recall that m,l, and q are the number of edges on the x,y, and z graphs, respectively. In addition, let X_k be a scalar from the vector $\tilde{\mathbf{X}}_k$ which indicates the scalar difference between x_i and x_j , corresponding to an edge on the x graph. Similarly, let Y_k (Z_k) be a scalar from the vector $\tilde{\mathbf{Y}}_k$ ($\tilde{\mathbf{Z}}_k$) defined by the corresponding y_i and y_j (z_i and z_j). Using this notation, the differences \mathbf{X}_{ij} on the RHS will now define the scalars $X_{ij} = x_j - x_i$, $Y_{ij} = y_j - y_i$, and $Z_{ij} = z_j - z_i$. Recall that (x_i, y_i, z_i) are the scalar coordinates of the individual oscillator, composing the network (2.1).

Using this notation, we can rewrite (9.21) as follows

$$n\left[\sum_{k=1}^{m} c_{k}X_{k}^{2} + \sum_{k=1}^{l} d_{k}Y_{k}^{2} + \sum_{k=1}^{q} g_{k}Z_{k}^{2}\right] >$$

$$961 \quad (9.22) \quad > a_{x}\sum_{i=1}^{n-1} \sum_{j>i,(i,j)\in C}^{n} X_{ij}^{2} + a_{y}\sum_{i=1}^{n-1} \sum_{j>i,(i,j)\in D}^{n} Y_{ij}^{2} + a_{z}\sum_{i=1}^{n-1} \sum_{j>i,(i,j)\in G}^{n} Z_{ij}^{2} + \sum_{i=1}^{n-1} \sum_{j>i,(i,j)\notin C,D,G}^{n} [\omega_{x}X_{ij}^{2} + \omega_{y}Y_{ij}^{2} + \omega_{z}Z_{ij}^{2}],$$

where $c_k = c_{i_k j_k}$, $d_k = d_{i_k j_k}$, and $g_k = g_{i_k j_k}$. Here, the RHS of (9.22) has four terms obtained by splitting the difference variables into four groups, according to the coefficients of A_{ij} (cf. (9.21) and (9.7)-(9.10)). The first sum on the RHS is composed of the differences that belong to the x graph C, the second sum corresponds to the y graph D, the third sum is defined by the z graph G, whereas the fourth sum identifies the differences between the oscillators which belong to different graphs such that, for example, $i \in C$ and $j \in D$.

To recalculate the difference variables of the RHS via the variables X_k , Y_k , and Z_k , we should first choose a path from oscillator i to oscillator j for any pair of oscillators (i,j). We denote this path by P_{ij} . Its path length $|P_{ij}|$ is the number of edges comprising the path. The important property of the path P_{ij} is that if, for example, it passes through oscillators with indices 1, 2, 3, and 4, then the corresponding difference $X_{14} = x_4 - x_1 = (x_4 - x_3) + (x_3 - x_2) + (x_2 - x_1) = X_{12} + X_{23} + X_{34}$, where the differences X_{12}, X_{23} , and X_{34} correspond to the edges and the path length $|P_{14}| = 3$.

The choice of paths is not unique. We typically choose a shortest path between any pair of i and j; however, a different choice of paths can yield closer estimates, as discussed in [11] for single-layer networks.

Once the choice of paths is made, we stick with it and begin recalculating the difference variables on the RHS of (9.22) via X_k , Y_k , and Z_k . A potential problem is that we have to deal not with the variables X_{ij} , but with their squares X_{ij}^2 , coming from the calculations of the derivative of the Lyapunov function (9.13). To mitigate this issue, we apply the Cauchy-Schwartz inequality; applied to the above example, it yields $X_{14}^2 = (X_{12} + X_{23} + X_{34})^2 \le 3(X_{12}^2 + X_{23}^2 + X_{34}^2)$. Notice the appearance of the factor 3, indicating the number of edges comprising the path. Similarly, for any difference X_{ij} , Y_{ij} , and Z_{ij} , we have

$$X_{ij}^{2} = \left(\sum_{k \in P_{ij}} X_{k}\right)^{2} \leq |P_{ij}| \sum_{k \in P_{ij}} X_{k}^{2},$$

$$Y_{ij}^{2} = \left(\sum_{k \in P_{ij}} Y_{k}\right)^{2} \leq |P_{ij}| \sum_{k \in P_{ij}} Y_{k}^{2},$$

$$Z_{ij}^{2} = \left(\sum_{k \in P_{ij}} Z_{k}\right)^{2} \leq |P_{ij}| \sum_{k \in P_{ij}} Z_{k}^{2},$$

where once again $|P_{ij}|$ indicates the length of the chosen path from oscillator i to oscillator j along the connection graph, combined of the x and y graphs. At this point, we do not differentiate between paths containing only x, y or z edges, but we have to consider interlayer paths when necessary.

Applying this idea to each difference variable on the RHS of (9.22), we obtain the following condition

$$n\left[\sum_{k=1}^{m} c_{k}X_{k}^{2} + \sum_{k=1}^{l} d_{k}Y_{k}^{2} + \sum_{k=1}^{q} g_{k}Z_{k}^{2}\right] > \sum_{k=1}^{m} [a_{x}b_{k}^{x} + \omega_{x}b_{k}^{int}]X_{k}^{2} + \sum_{j=1}^{l} [a_{y}b_{k}^{y} + \omega_{y}b_{k}^{int}]Y_{k}^{2} + \sum_{j=1}^{q} [a_{z}b_{k}^{z} + \omega_{z}b_{k}^{int}]Z_{k}^{2} + \sum_{j=1}^{q} [\omega_{x}b_{k}^{int}]X_{k}^{2} + \sum_{j=1}^{q} [\omega_{x}b_{k}^{int}]Y_{k}^{2} + \sum_{j=1}^{q} [\omega_{z}b_{k}^{int}]Z_{k}^{2},$$

where $b_k^x = \sum_{j>i; k \in P_{ij} \in C}^n |P_{ij}|$ is the sum of the lengths of all chosen paths which belong

996 to the x graph C and go through a given x edge k. Similarly, $b_k^y = \sum_{j>i; k \in P_{ij} \in D}^n |P_{ij}|$

 $(b_k^z = \sum_{j>i; k \in P_{ij} \in G}^n |P_{ij}|)$ is the sum of the lengths of all chosen paths which belong

to the y graph D (z graph G) and go through a given y (z) edge k. Finally, $b_k^{int} = \sum_{j>i;\ k\in P_{ij}:(i,j)\notin C,D,G} |P_{ij}|$ is the sum of the lengths of all chosen paths between pairs

of nodes i and j which belong to two different graphs and are composed from more than one type of edge and go through a given edge k which may be an x, y or z edge.

Note that the three sums on the LHS of (9.24) correspond to the first three sums on the RHS. In the simplest case where all three C, D, and G graphs are connected such that each graph couples all n oscillators, b_k^{int} can always be set to 0, since there are always paths between any two nodes that entirely belong to either of the three x, y, and z graphs. As a result, the last three sums on the RHS disappear, and we immediately obtain the stability conditions by dropping the summation signs and the difference variables

1009 (9.25)
$$c_k + d_k + g_k > \frac{1}{n} \left\{ a_x b_k^x + a_y b_k^y + a_z b_k^z \right\}.$$

In the case of disconnected graphs C, D, and G where all oscillators are coupled through a combination of two or three graphs and b_k^{int} is non-zero, at least two of the last three sums are always present on the RHS. This makes the argument much more complicated but yields a number of surprising implications of the stability method to specific networks discussed in Sections 5 and 6.

A major stability problem, associated with the last three terms is rooted in the fact that, for example, the fourth sum $\sum_{k\in D\cup G} [\omega_x b_k^{int}] X_k^2$ contains the difference variables X_k that correspond to the edges of the y or z graph. As a result, the first sum $n\sum_{k=1}^m c_k X_k^2$ on the LHS which contains the variables X_k that correspond to x edges, cannot compensate the fourth sum on the RHS as they belong to different graphs and therefore cannot be compared. At the same time, the second (third) sum $n\sum_{k=1}^{l} d_k Y_k^2$

 $\left(n\sum_{k=1}^q g_k Z_k^2\right)$ on the LHS does belong to the y (z) graph but contains the variables Y_k (Z_k) and not X_k needed to handle the fourth sum on the RHS. The same problem relates to the last two sums $\sum_{k\in C\cup G} [\omega_y b_k^{int}] Y_k^2$ and $\sum_{k\in C\cup D} [\omega_z b_k^{int}] Z_k^2$ which contain Y_k and Z_k variables, respectively and correspond to the "wrong" graphs.

How can we get around this problem as we simply do not have means on the LHS to compensate for the troublesome sums on the RHS? A solution comes from economics: if you do not have means, borrow them! [But act responsibly]. This remark is added to entertain the reader that might be tired of following the proof up to this point.

In fact, the only place to "borrow" these terms from is the auxiliary stability systems (9.7), (9.8), and (9.9) as they do contain the desired variables X_k , Y_k , and Z_k , corresponding to the "right" graphs (the x, y, and z graphs, respectively). Therefore, we need to go back and modify the auxiliary systems (9.7), (9.8), and (9.9) as follows

$$\dot{\mathbf{X}}_{ij} = \begin{bmatrix} \int_{0}^{1} D\mathbf{F}(v\mathbf{x}_{j} + (1-v)\mathbf{x}_{i}) dv - [a_{x} + \alpha_{x}^{k}]P + \\ +\omega_{y}b_{k}^{int}L + \omega_{z}b_{k}^{int}M \end{bmatrix} \mathbf{X}_{ij} \text{ if } i, j \in x\text{-edge } k,$$

1036 (9.27) $\dot{\mathbf{X}}_{ij} = \begin{bmatrix} \int_{0}^{1} D\mathbf{F}(v\mathbf{x}_{j} + (1-v)\mathbf{x}_{i}) dv - (a_{y} + \alpha_{y}^{k})L + \omega_{x}b_{k}^{int}P + \omega_{z}b_{k}^{int}M \end{bmatrix} \mathbf{X}_{ij} \text{ if } i, j \in y\text{-edge } k.$

$$\dot{\mathbf{X}}_{ij} = \begin{bmatrix} \int_{0}^{1} D\mathbf{F}(v\mathbf{x}_{j} + (1-v)\mathbf{x}_{i}) dv - (a_{z} + \alpha_{z}^{k})G + \omega_{x}b_{k}^{int}P + \omega_{y}b_{k}^{int}L \end{bmatrix} \mathbf{X}_{ij} \text{ if } i, j \in z\text{-edge } k.$$

The addition of positive terms $\omega_y b_k^{int} L \mathbf{X}_{ij}$ and $\omega_z b_k^{int} M \mathbf{X}_{ij}$ to the auxiliary system (9.26) worsens its stability, therefore we have to introduce an additional parameter α_x^k and make sure that it is sufficiently large to stabilize the new auxiliary system. A very important property is that, in (9.26), we have to add the positive, destabilizing term $\omega_y b_k^{int} L X_{ij}$ to the second equation for the $(y_j - y_i)$ difference and the positive, destabilizing term $\omega_z b_k^{int} M X_{ij}$ to the third equation for the $(z_j - z_i)$ difference but try to stabilize the system via increasing the additional parameter α_x^k in the first equation

for the $(x_j - x_i)$ equation (note the different inner matrices: P versus L and M in (9.26)). Depending on the individual oscillator, chosen as the individual unit, this might not be possible, especially when traffic load b_k^{int} on the edge k is high. This property is discussed in detail for the Lorenz and double scroll oscillator examples in Sections 5 and 6. A similar argument carries over to the auxiliary systems (9.27) and (9.28) where, for example in (9.27), we add the destabilizing terms $\omega_x b_k^{int} P \mathbf{X}_{ij}$ and $\omega_z b_k^{int} M \mathbf{X}_{ij}$ to the $(x_j - x_i)$ and $(z_j - z_i)$ equations, respectively, but seek to stabilize the system via the additional parameter α_y^k in the $(y_j - y_i)$ equation.

Notice that we only modify the auxiliary systems for the existing x, y, and z edges. All the other auxiliary systems for \mathbf{X}_{ij} , that do not correspond to edges of either of the x, y and z graphs, remain intact and defined via the original systems (9.7)-(9.10). Thus, the modifications of (9.26), (9.27), and (9.28) make the troublesome sums $\sum_{k \in D \cup G} [\omega_x b_k^{int}] X_k^2, \sum_{k \in C \cup G} [\omega_y b_k^{int}] Y_k^2, \text{ and } \sum_{k \in C \cup D} [\omega_z b_k^{int}] Z_k^2 \text{ in (9.24) disappear at the expense of worsened stability conditions of the corresponding auxiliary systems, which is reflected by the appearance of additional terms with <math>\alpha_x^k$, α_y^k , and α_z^k . Therefore, (9.24) turns into

(9.29)

1054

1056

1057 1058

1061

1078 1079

$$n\left[\sum_{k=1}^{m} c_{k}X_{k}^{2} + \sum_{k=1}^{l} d_{k}Y_{k}^{2} + \sum_{k=1}^{q} g_{k}Z_{k}^{2}\right] > \sum_{k=1}^{m} [a_{x}b_{k}^{x} + \omega_{x}b_{k}^{int} + \alpha_{x}^{k}]X_{k}^{2} + \sum_{k=1}^{l} [a_{y}b_{k}^{y} + \omega_{y}b_{k}^{int} + \alpha_{y}^{k}]Y_{k}^{2} + \sum_{k=1}^{q} [a_{z}b_{k}^{z} + \omega_{z}b_{k}^{int} + \alpha_{z}^{k}]Z_{k}^{2}.$$

Notice the new stabilizing constants α_x^k , α_y^k , and α_z^k . Depending on the individual oscillator dynamics and traffic load on edge k, these constants might have to be very large or even infinite.

Comparing the terms containing X_k , Y_k , and Z_k on the LHS and RHS of (9.29) and omitting the summation signs, we obtain the following conditions

$$nc_{k}X_{k}^{2} > [a_{x}b_{k}^{x} + \omega_{x}b_{k}^{int} + \alpha_{x}^{k}]X_{k}^{2}, \quad k = 1, ..., m,$$

$$nd_{k}Y_{k}^{2} > [a_{y}b_{k}^{y} + \omega_{y}b_{k}^{int} + \alpha_{y}^{k}]Y_{k}^{2}, \quad k = 1, ..., l,$$

$$ng_{k}Z_{k}^{2} > [a_{z}b_{k}^{z} + \omega_{z}b_{k}^{int} + \alpha_{z}^{k}]Z_{k}^{2}, \quad k = 1, ..., q.$$

Finally, we omit the difference variables to obtain the bounds on coupling strengths, c_k for x edges, d_k for y edges, and g_k for z edges, sufficient to make the derivative of the Lyapunov function (9.13) negative semi-definite, and therefore, ensure global stability of synchronization in the network (2.1). It follows from (9.30) that these upper bounds are

$$c_{k} > \frac{1}{n} [a_{x}b_{k}^{x} + \omega_{x}b_{k}^{int} + \alpha_{x}^{k}], \quad k = 1, ..., m,$$

$$d_{k} > \frac{1}{n} [a_{y}b_{k}^{y} + \omega_{y}b_{k}^{int} + \alpha_{y}^{k}], \quad k = 1, ..., l,$$

$$g_{k} > \frac{1}{n} [a_{z}b_{k}^{z} + \omega_{z}b_{k}^{int} + \alpha_{z}^{k}], \quad k = 1, ..., q.$$

1075 This completes the proof of Theorem 4.1. \square

1076 REFERENCES

- J AGUIRRE, R SEVILLA-ESCOBOZA, R GUTIÉRREZ, D PAPO, AND JM BULDÚ, Synchronization of interconnected networks: the role of connector nodes, Physical Review Letters, 112 (2014), p. 248701.
- 1080 [2] RÉKA ALBERT AND ALBERT-LÁSZLÓ BARABÁSI, Statistical mechanics of complex networks, Re-1081 views of Modern Physics, 74 (2002), p. 47.

1082 [3] MAURICIO BARAHONA AND LOUIS M PECORA, Synchronization in small-world systems, Physical 1083 Review Letters, 89 (2002), p. 054101.

1087

1088

1089

1090

1091

1092

1093

1094

1095

1096

1097 1098

1099

1100

1101

1102

1103

1104

1105

1106 1107

1108

1109

1110

1111

1112

1113

1114

1115

1116

1117

1118 1119

1120

1121

1122

1123

1124

1125

1131

1135 1136

1139

- 1084 [4] IGOR BELYKH, VLADIMIR BELYKH, AND MARTIN HASLER, Blinking model and synchronization 1085 in small-world networks with a time-varying coupling, Physica D: Nonlinear Phenomena, 1086 195 (2004), pp. 188-206.
 - Generalized connection graph method for synchronization in asymmetrical networks, Physica D: Nonlinear Phenomena, 224 (2006), pp. 42-51.
 - , Synchronization in asymmetrically coupled networks with node balance, Chaos: An Interdisciplinary Journal of Nonlinear Science, 16 (2006), p. 015102.
 - [7] IGOR BELYKH, ENNO DE LANGE, AND MARTIN HASLER, Synchronization of bursting neurons: What matters in the network topology, Physical Review Letters, 94 (2005), p. 188101.
 - [8] IGOR BELYKH, MARIO DI BERNARDO, JÜRGEN KURTHS, AND MAURIZIO PORFIRI, Evolving dynamical networks, Physica D: Nonlinear Phenomena, 267 (2014), pp. 1–6.
 - [9] IGOR BELYKH AND MARTIN HASLER, Mesoscale and clusters of synchrony in networks of bursting neurons, Chaos: An Interdisciplinary Journal of Nonlinear Science, 21 (2011),
 - [10] IGOR BELYKH, MARTIN HASLER, AND VLADIMIR BELYKH, When symmetrization guarantees synchronization in directed networks, International Journal of Bifurcation and Chaos, 17 (2007), pp. 3387-3395.
 - [11] IGOR BELYKH, MARTIN HASLER, MENNO LAURET, AND HENK NIJMEIJER, Synchronization and graph topology, International Journal of Bifurcation and Chaos, 15 (2005), pp. 3423–3433.
 - [12] IGOR BELYKH, RUSSELL JETER, AND VLADIMIR BELYKH, Foot force models of crowd dynamics on a wobbly bridge, Science Advances, 3 (2017), p. e1701512.
 - [13] IGOR BELYKH, REIMBAY REIMBAYEV, AND KUN ZHAO, Synergistic effect of repulsive inhibition $in\ synchronization\ of\ excitatory\ networks,\ Physical\ Review\ E,\ 91\ (2015),\ p.\ 062919.$
 - [14] IGOR BELYKH AND ANDREY SHILNIKOV, When weak inhibition synchronizes strongly desynchronizing networks of bursting neurons, Physical Review Letters, 101 (2008), p. 078102.
 - [15] IGOR V BELYKH, RUSSELL JETER, AND VLADIMIR N BELYKH, Bistable gaits and wobbling induced by pedestrian-bridge interactions, Chaos: An Interdisciplinary Journal of Nonlinear Science, 26 (2016), p. 116314.
 - [16] VLADIMIR N BELYKH, IGOR V BELYKH, AND MARTIN HASLER, Connection graph stability method for synchronized coupled chaotic systems, Physica D: Nonlinear Phenomena, 195 (2004), pp. 159-187.
 - [17] VLADIMIR N BELYKH, NIKOLAI N VERICHEV, LJUPCO KOCAREV, AND LEON CHUA, On chaotic synchronization in a linear array of chua's circuits, Journal of Circuits, Systems, and Computers, 3 (1993), pp. 579-590.
 - [18] KAREN A BLAHA, KE HUANG, FABIO DELLA ROSSA, LOUIS PECORA, MANI HOSSEIN-ZADEH, AND FRANCESCO SORRENTINO, Cluster synchronization in multilayer networks: A fully analog experiment with lc oscillators with physically dissimilar coupling, Physical Review Letters, 122 (2019), p. 014101.
 - [19] STEFANO BOCCALETTI, GINESTRA BIANCONI, REGINO CRIADO, CHARO I DEL GENIO, JESÚS GÓMEZ-GARDENES, MIGUEL ROMANCE, IRENE SENDINA-NADAL, ZHEN WANG, AND MASSI-MILIANO ZANIN, The structure and dynamics of multilayer networks, Physics Reports, 544 (2014), pp. 1–122.
- 1126 [20] STEFANO BOCCALETTI, JÜRGEN KURTHS, GRIGORY OSIPOV, DL VALLADARES, AND CS ZHOU, 1127 The synchronization of chaotic systems, Physics Reports, 366 (2002), pp. 1–101.
- 1128 [21] STEFANO BOCCALETTI, VITO LATORA, YAMIR MORENO, MARTIN CHAVEZ, AND D-U HWANG, 1129 Complex networks: Structure and dynamics, Physics Reports, 424 (2006), pp. 175-308.
- 1130 [22] JOHN BUCK AND ELISABETH BUCK, Synchronous fireflies, Scientific American, 234 (1976), pp. 74-85.
- [23] SERGEY V BULDYREV, RONI PARSHANI, GERALD PAUL, H EUGENE STANLEY, AND SHLOMO 1132 1133 HAVLIN, Catastrophic cascade of failures in interdependent networks, Nature, 464 (2010), 1134
 - [24] Guanrong Chen and Y Xinghuo, Chaos Control Theory and Applications Series: Lecture Notes in Control and Information Sciences, vol. 292, Springer, 2003.
- 1137 [25] James J Collins and Ian N Stewart, Coupled nonlinear oscillators and the symmetries of 1138 animal gaits, Journal of Nonlinear Science, 3 (1993), pp. 349-392.
 - [26] MANLIO DE DOMENICO, CLARA GRANELL, MASON A PORTER, AND ALEX ARENAS, The physics of spreading processes in multilayer networks, Nature Physics, 12 (2016), p. 901.
- 1141 [27] Charo I del Genio, Jesús Gómez-Gardeñes, Ivan Bonamassa, and Stefano Boccaletti, 1142 Synchronization in networks with multiple interaction layers, Science Advances, 2 (2016), 1143p. e1601679.

- 1144 [28] EDSGER W DIJKSTRA, A note on two problems in connexion with graphs, Numerische mathe-1145 matik, 1 (1959), pp. 269–271.
- 1146 [29] Bruno Eckhardt, Edward Ott, Steven H Strogatz, Daniel M Abrams, and Allan McRobie, Modeling walker synchronization on the Millennium Bridge, Physical Review E, 75 (2007), p. 021110.
- [30] LEON GLASS AND MICHAEL C MACKEY, From Clocks to Chaos: the Rhythms of Life, Princeton
 University Press, 1988.

1154

1155

1156

 $1157 \\ 1158$

1159

1160

1161

1162

1163

1164

1168

1169

 $1170 \\ 1171$

1172

1173

1174

 $1175 \\ 1176$

1177

1178

1179

1184

1185

1186

- 1151 [31] OLGA GOLOVNEVA, RUSSELL JETER, IGOR BELYKH, AND MAURIZIO PORFIRI, Windows of op-1152 portunity for synchronization in stochastically coupled maps, Physica D: Nonlinear Phe-1153 nomena, 340 (2017), pp. 1–13.
 - [32] MICHAEL R GUEVARA, ALVIN SHRIER, AND LEON GLASS, Phase-locked rhythms in periodically stimulated heart cell aggregates, American Journal of Physiology - Heart and Circulatory Physiology, 254 (1988), pp. H1–H10.
 - [33] JAMES F HEAGY, LOUIS M PECORA, AND THOMAS L CARROLL, Short wavelength bifurcations and size instabilities in coupled oscillator systems, Physical Review Letters, 74 (1995), p. 4185.
 - [34] James L Hindmarsh and RM Rose, A model of neuronal bursting using three coupled first order differential equations, Proceedings of the Royal society of London. Series B. Biological sciences, 221 (1984), pp. 87–102.
 - [35] J HONERKAMP, The heart as a system of coupled nonlinear oscillators, Journal of Mathematical Biology, 18 (1983), pp. 69–88.
- 1165 [36] Daniel Irving and Francesco Sorrentino, Synchronization of dynamical hypernetworks:
 1166 Dimensionality reduction through simultaneous block-diagonalization of matrices, Physical
 1167 Review E, 86 (2012), p. 056102.
 - [37] RUSSELL JETER AND IGOR BELYKH, Synchronization in on-off stochastic networks: windows of opportunity, IEEE Transactions on Circuits and Systems I: Regular Papers, 62 (2015), pp. 1260–1269.
 - [38] MIKKO KIVELÄ, ALEX ARENAS, MARC BARTHELEMY, JAMES P GLEESON, YAMIR MORENO, AND MASON A PORTER, Multilayer networks, Journal of Complex Networks, 2 (2014), pp. 203– 271.
 - [39] NANCY KOPELL AND BARD ERMENTROUT, Chemical and electrical synapses perform complementary roles in the synchronization of interneuronal networks, Proceedings of the National Academy of Sciences of the United States of America, 101 (2004), pp. 15482–15487.
 - [40] ZHI LI AND GUANRONG CHEN, Global synchronization and asymptotic stability of complex dynamical networks, IEEE Transactions on Circuits and Systems II: Express Briefs, 53 (2006), pp. 28–33.
- 1180 [41] EDWARD N LORENZ, Deterministic nonperiodic flow, Journal of the Atmospheric Sciences, 20 (1963), pp. 130–141.
- [42] RABINDER N MADAN, Chua's Circuit: a Paradigm for Chaos, World Scientific Publishing, 1993.
 [43] ADILSON E. MOTTER, SETH A. MYERS, MARIAN ANGHEL, AND TAKASHI NISHIKAWA, Sponta-
 - [43] ADILSON E. MOTTER, SETH A. MYERS, MARIAN ANGHEL, AND TAKASHI NISHIKAWA, Spontaneous synchrony in power-grid networks, Nature Physics, 9 (2013), p. 191.
 - [44] HIROYA NAKAO, TATSUO YANAGITA, AND YOJI KAWAMURA, Phase-reduction approach to synchronization of spatiotemporal rhythms in reaction-diffusion systems, Physical Review X, 4 (2014), p. 021032.
- 1188 [45] Theoden I Netoff and Steven J Schiff, Decreased neuronal synchronization during exper-1189 inental seizures, Journal of Neuroscience, 22 (2002), pp. 7297–7307.
- 1190 [46] MARK EJ NEWMAN, The structure and function of complex networks, SIAM Review, 45 (2003), 1191 pp. 167–256.
- 1192 [47] TAKASHI NISHIKAWA AND ADILSON E MOTTER, Network synchronization landscape reveals com-1193 pensatory structures, quantization, and the positive effect of negative interactions, Pro-1194 ceedings of the National Academy of Sciences, 107 (2010), pp. 10342–10347.
- 1195 [48] Takashi Nishikawa, Jie Sun, and Adilson E Motter, Sensitive dependence of optimal net-1196 work dynamics on network structure, Physical Review X, 7 (2017), p. 041044.
- [49] LOUIS M PECORA AND THOMAS L CARROLL, Master stability functions for synchronized coupled systems, Physical Review Letters, 80 (1998), p. 2109.
- 1199 [50] Arkady Pikovsky, Michael Rosenblum, and Jürgen Kurths, Synchronization: a Universal 2000 Concept in Nonlinear Sciences, vol. 12, Cambridge University Press, 2003.
- 1201 [51] MAURIZIO PORFIRI AND IGOR BELYKH, Memory matters in synchronization of stochastically 202 coupled maps, SIAM Journal on Applied Dynamical Systems, 16 (2017), pp. 1372–1396.
- 1203 [52] MAURIZIO PORFIRI AND DANIEL J STILWELL, Consensus seeking over random weighted directed graphs, IEEE Transactions on Automatic Control, 52 (2007), pp. 1767–1773.
- 1205 [53] MAURIZIO PORFIRI, DANIEL J STILWELL, ERIK M BOLLT, AND JOSEPH D SKUFCA, Random

- 1206 talk: Random walk and synchronizability in a moving neighborhood network, Physica D: 1207 Nonlinear Phenomena, 224 (2006), pp. 102-113.
- 1208 [54] FILIPPO RADICCHI AND GINESTRA BIANCONI, Redundant interdependencies boost the robustness 1209 of multiplex networks, Physical Review X, 7 (2017), p. 011013.
 - [55] REIMBAY REIMBAYEV, KEVIN DALEY, AND IGOR BELYKH, When two wrongs make a right: synchronized neuronal bursting from combined electrical and inhibitory coupling, Phil. Trans. R. Soc. A, 375 (2017), p. 20160282.
 - [56] Paul So, Bernard C Cotton, and Ernest Barreto, Synchronization in interacting populations of heterogeneous oscillators with time-varying coupling, Chaos: An Interdisciplinary Journal of Nonlinear Science, 18 (2008), p. 037114.
- 1216 [57] Francesco Sorrentino, Synchronization of hypernetworks of coupled dynamical systems, New 1217 Journal of Physics, 14 (2012), p. 033035.
- 1218 [58] Francesco Sorrentino and Edward Ott, Adaptive synchronization of dynamics on evolving 1219 complex networks, Physical Review Letters, 100 (2008), p. 114101. 1220
 - [59] Steven H Strogatz, Exploring complex networks, Nature, 410 (2001), p. 268.

1210

1211 1212

1213

1214

1215

1221

1222

1223

1224

1225

1226

1227

1228

1229

1230

1231

1232

1233

12341235

1236

1237 1238

1239

1240

1241

- [60] STEVEN H STROGATZ, DANIEL M ABRAMS, ALLAN MCROBIE, BRUNO ECKHARDT, AND EDWARD Ott, Theoretical mechanics: Crowd synchrony on the Millennium Bridge, Nature, 438 (2005), pp. 43-44.
- [61] JIE SUN, ERIK M BOLLT, AND TAKASHI NISHIKAWA, Master stability functions for coupled nearly identical dynamical systems, Europhysics Letters, 85 (2009), p. 60011.
- [62] DANE TAYLOR, SARAY SHAI, NATALIE STANLEY, AND PETER J MUCHA, Enhanced detectability of community structure in multilayer networks through layer aggregation, Physical Review Letters, 116 (2016), p. 228301.
- [63] VINCENT TORRE, A theory of synchronization of heart pace-maker cells, Journal of Theoretical Biology, 61 (1976), pp. 55-71.
- [64] XIAO FAN WANG AND GUANRONG CHEN, Synchronization in scale-free dynamical networks: robustness and fragility, IEEE Transactions on Circuits and Systems I: Fundamental Theory and Applications, 49 (2002), pp. 54-62.
- [65] Chai Wah Wu, Synchronization in Coupled Chaotic Circuits & Systems, vol. 41, World Scientific, 2002.
- [66]-, Synchronization and convergence of linear dynamics in random directed networks, IEEE Transactions on Automatic Control, 51 (2006), pp. 1207–1210.
- [67] CHAI WAH WU AND LEON O CHUA, On a conjecture regarding the synchronization in an array of linearly coupled dynamical systems, IEEE Transactions on Circuits and Systems I: Fundamental Theory and Applications, 43 (1996), pp. 161–165.
- [68] LIYUE ZHANG, ADILSON E MOTTER, AND TAKASHI NISHIKAWA, Incoherence-mediated remote synchronization, Physical Review Letters, 118 (2017), p. 174102.
- 1243 [69] XIYUN ZHANG, STEFANO BOCCALETTI, SHUGUANG GUAN, AND ZONGHUA LIU, Explosive syn-1244chronization in adaptive and multilayer networks, Physical Review Letters, 114 (2015), 1245 p. 038701.